IEEE Access
Multidisciplinary | Rapid Review | Open Access Journal

Received July 9, 2019, accepted August 1, 2019, date of publication August 5, 2019, date of current version August 19, 2019.

Digital Object Identifier 10.1109/ACCESS.2019.2933173

A Comprehensive Survey on UAV Communication Channel Modeling

CHAOXING YAN[1], (Member, IEEE), LINGANG FU[1], JIANKANG ZHANG[2], (Senior Member, IEEE), AND JINGJING WANG[3], (Member, IEEE)

[1]Beijing Research Institute of Telemetry, Beijing 100076, China
[2]Electronics and Computer Science, University of Southampton, Southampton SO17 1BJ, U.K.
[3]Department of Electrical Engineering, Tsinghua University, Beijing 100084, China

Corresponding author: Chaoxing Yan (chaoxingyan@foxmail.com)

This work was supported by the Key Project of the Key Research and Development Program, Ministry of Science and Technology, China, under Grant 2018YFC1407200 and Grant 2017YFC1405200.

ABSTRACT Unmanned aerial vehicles (UAVs) have stroke great interested both by the academic community and the industrial community due to their diverse military applications and civilian applications. Furthermore, UAVs are also envisioned to be part of future airspace traffic. The application functions delivery relies on information exchange among UAVs as well as between UAVs and ground stations (GSs), which further closely depends on aeronautical channels. However, there is a paucity of comprehensive surveys on aeronautical channel modeling in line with the specific aeronautical characteristics and scenarios. To fill this gap, this paper focuses on reviewing the air-to-ground (A2G), ground-to-ground (G2G), and air-to-air (A2A) channel measurements and modeling for UAV communications and aeronautical communications under various scenarios. We also provide the design guideline for managing the link budget of UAV communications taking account of link losses and channel fading effects. Moreover, we also analyze the receive/transmit diversity gain and spatial multiplexing gain achieved by multiple-antenna-aided UAV communications. Finally, we discuss the remaining challenge and open issues for the future development of UAV communication channel modeling.

INDEX TERMS UAV communication, aeronautical communication, channel characterization, statistical channel, air-to-ground, cellular networks, evaporation duct, shadowing, MIMO.

I. INTRODUCTION

Benefiting from the technical advances in artificial intelligence, computer and sensor technology, the world has seen the high profile of advanced military unmanned aerial vehicles (UAVs), such as Predator, and Global hawk [1]. Along with the progress of embedded systems, low-power long-range radio devices, inexpensive airframes and the miniaturization of micro-electro-mechanical systems (MEMS), UAVs have also become affordable for hitherto unexplored scientific and commercial applications. The past couple of years have been pivotal in bringing UAVs further to personal drones, such as the Mavic, Phantom and Inspire from DJI [2], the AR and Bebop from Parrot [3], and the Solo from 3D Robotics [4]. As part of Google Project Loon, high altitude and large-scale UAV long term evolution (LTE) eNodeBs were proposed as alternatives for terrestrial eNodeBs. When UAVs are combined with ground control stations and data links, it forms a UAS (Unmanned Aerial System). UAS must be considered in a system context which includes the command, control and communication (C3) system. For the aerial networks of space-air-ground integrated network [5], [6], UAVs, airships and balloons are three primary infrastructures for constructing the hybrid aerial mobile system. Generally, large UAVs, airships, and balloons constitute the high-altitude platforms (HAPs), while low-altitude platforms (LAPs) are dominated by cooperative small drones. The use of UAVs and other aerial devices for relay links is an emerging technology and hence requires the channel to be characterized for establishing communication links, which can be broadly classified into two aspects namely, air-to-ground (A2G) communications and air-to-air (A2A) communications.

The associate editor coordinating the review of this manuscript and approving it for publication was Jiayi Zhang.

A. UAV CLASSIFICATIONS

The UAVs differ one to each other for size and structure. The most common factors for UAV classification in the literature are maximum takeoff weight, operational altitude, level of control autonomy, launch method, ownership, and airspace class [7]–[10]. Based on the cruise-duration and action-radius, UAVs were also categorized into four kinds [11]: high-altitude and long-endurance UAVs, medium range UAVs, low-cost and short-range small UAVs, and mini drones. From the view of communication capability, the radius range of UAV data link plays an important role in our classification, which is given as,

1) Long-endurance UAVs are applied in reconnaissance, interception or attack, as exemplified by the CH-4, Predator, EuroHawk, and Global Hawk UAVs [1].
2) Mid-range UAVs have an action radius of about 650 km, being primarily designed for mid-range reconnaissance and combat effect assessment [12].
3) Short-range small UAVs have an action radius of less than 350 km, such as the British Phoenix, Israeli Scout UAVs [13]. Their flight altitude is less than 3 km and flight span is about 8-12 hours.
4) Close-range UAVs have a more limited cruising duration spanning from 1 hour to 6 hours depending on the mission, and provide coverage of at least 30 km.
5) Very low cost close-range UAVs have a flight-span of about 5 km. The AeroVironment Raven and the Dragon Eye represent this type of UAVs [14].
6) Commercial and consumer UAVs have very limited range using remote control console or can be controlled even by an ''App'' on a smart phone or tablet computer and bring forth the age of ''drones'' with tremendous commercial potentials.

There are striking difference between UAV and commercial aeronautical communications, whereas there are more similarities between UAV and aeronautical communications, considering the diverse range of categories of UAVs.

- Most channel measurements for civil aeronautical communication employ manned aircrafts, which often require airports for takeoff and landing. Civil aeronautical communication also requires a high enough flight altitude and long enough distance to take slight maneuvering. The aeronautical channel would lay the foundation for UAV link designs in that most military or industrial UAVs are also located at an airport.
- UAV communication channel measurements have diverse aircraft sizes, which ensure their flight height reach down to tens of meters for mini-UAV, or up to thousands of meters for the UAV taking off from an airport and flying like an airplane. The former one can operate with forced turning maneuvering, whereas the later one can work at severe environments resulting in channels similar to aeronautical channel.

Zhang *et al.* [15] gave an overview of aeronautical communication, and clarified that mobile ad hoc network (MANET) included ad hoc networks mobile users, vehicles and UAVs as well as airplanes, whereas the specific vehicular ad hoc networks (VANETs), flying ad hoc networks (FANETs) and aeronautical ad-hoc networks (AANETs) would refer to the networks constituted by vehicles, UAVs and airplanes, respectively.

B. RELATED WORKS

Bello investigated the aeronautical channel between aircraft and satellites [16], and Haas devoted his efforts to A2G and A2A aeronautical channel models [17]. The very first aeronautical data communications system is aircraft communications addressing and reporting (ACARS) [18]. Hughes network systems developed the extended time division multiple access (TDMA) datalink, which was used in L-band digital aeronautical communication system (L-DACS), covering airport surface, continental, oceanic and remote communications with two candidate systems named L-DACS1 and L-DACS2. Two parallel programs are working toward the definition of a new air traffic management (ATM) system [19]: the single European sky ATM research (SESAR) program in Europe and the next generation air transportation system (NextGen) program in the United States.

During the UAS integration project in the national airspace system by NASA Glenn research center, Matolak and Sun [20]–[22] classified their UAV channel measurements by terrain types: flat, hilly, mountainous, and over water. Their study in [23] presented a brief review of UAS air-ground channels in approximately chronological order while neglecting references to bands well outside L- and C-bands. Elston *et al.* [24] developed a net-centric communication, command, and control architecture using WiFi network [25] for a heterogeneous UAS comprised of small and miniature unmanned aircraft. Bekmezci *et al.* [26] proposed the multiple-UAV system based on the concept of FANET. Khuwaja *et al.* [27] provided a survey on the measurement methods for UAV channel modeling using low altitude platforms and classified it into deterministic models, tapped delay line (TDL) model and geometric-based stochastic models. Khawaja *et al.* [28] recently conducted a survey on the A2G channel measurement campaigns, large and small scale fading channel models.

However, there is a paucity of comprehensive surveys on both aerial and aeronautical channel modeling taking into account their specific characteristics, scenarios, and challenges. In this paper, we will review the UAV and aeronautical communication channel modeling studies. Compared to existing channel modeling survey works on LAPs [27] and A2G channels [28], this comprehensive survey commences with UAV link budget, and then reviews aeronautical and UAV channels for diverse aircrafts and scenarios. We emphasize G2G and A2A channels in addition to conventional A2G channels [28]. we also provide the overview of ducting, aircraft shadowing and MIMO (multiple-input multiple-output) channels in UAV communications. We include a timeline representation of these channel measurements and studies in Fig. 1, where the list of references is not intended to

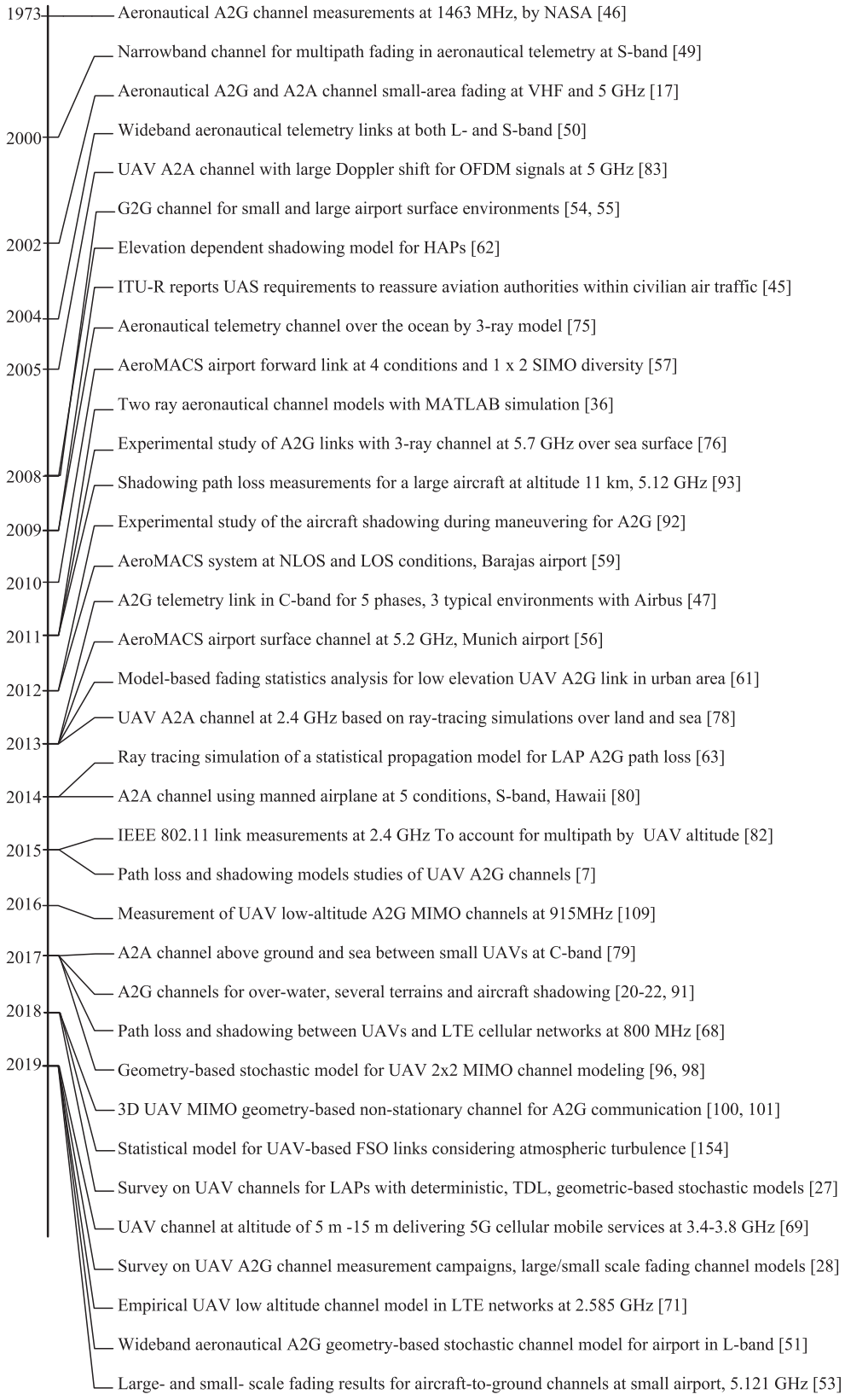

FIGURE 1. **Timeline of channel modeling for UAV and civil aeronautical communications.**

be exhaustive. From this timeline, we find that the UAV channel measurements have come into bloom during the last 10 years. In addition, the experimental results in [29] show that the geostationary Earth orbit (GEO) satellite channel behaves like Rician fading during normal flight situations and maneuvers with a Rice factor above 20 dB. LOS conditions can be assumed and the channel can be fairly approximated by an additive white Gaussian noise (AWGN) channel for most of the time. Therefore, the satellite communications channels via either GEO or LEO satellites are not considered in the following text.

The organization of rest of the paper is as follows. In Section II, we generally analyze the UAV communication link budget and channel fadings. In Section III, we review the channel modeling and measurements for aeronautical communications. In Section IV, we overview the UAV communication channels for A2G and A2A links, duct as well as shadowing. The UAV channels in the context of multiple antenna techniques are investigated in Section V. The potential challenges and open issues of UAV channel modeling are discussed in Section VI. Finally, we draw conclusions in Section VII. The organization of this paper is shown at a glance in Fig. 2.

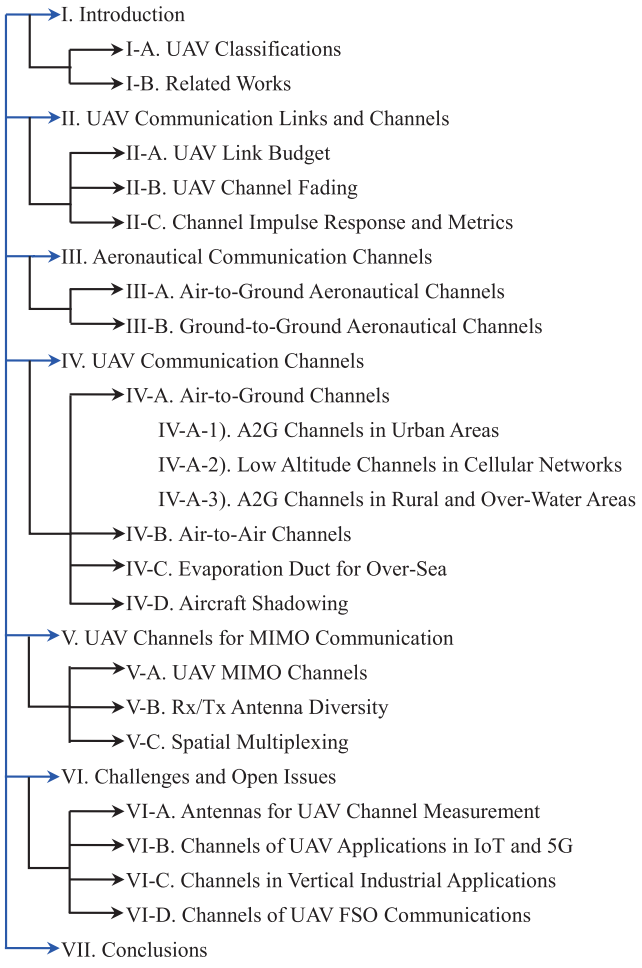

FIGURE 2. The outline of this paper.

II. UAV COMMUNICATION LINKS AND CHANNELS

The international civil aviation organization (ICAO) decides that UAV control and nonpayload communication (CNPC) links must operate over protected spectrum. To regulate the UAV applications, international telecommunication union (ITU) has allowed the use of certain portions of the L-band: 960 MHz – 977 MHz and C-band: 5030 MHz – 5091 MHz for UAS CNPC link [30]. The Ku-band downlink: 10.95 GHz – 12.75 GHz and uplink: 14.0 GHz – 14.47 GHz, and Ka-band downlink: 19.70 GHz – 20.20 GHz and uplink: 29.5 GHz – 30 GHz are authorized for beyond line-of-sight (BLOS) CNPC spectrum of satellite aeronautical safety communications. The bands of 840.5 MHz – 845 MHz, 1430 MHz – 1444 MHz, and 2408 MHz – 2440 MHz have been approved for unmanned aircraft systems relying on LOS links by China [5], [31].

NASA has supported major UAV projects designed for terrestrial as well as space missions [32]. Jet Propulsion Laboratory (JPL) developed UAV communications payload for high-rate X-band links and for battlefield broadcast in the S-band [33], supporting a maximum data rate of 45 Mbps over a range up to 100 miles in the context of full duplex links. The communication capability of aircraft will be affected by the altitude, range, receiver sensitivity, transmitter power, antenna type, coax type and length, as well as the terrain details. Lee [34] designed the UAV link budget of long-distance 200 km for Ku-band LOS wireless link at average altitude of 3 km. They calculate the system carrier-to-noise ratio (C/N) taking account of free space loss (FSL) for different geography and weather. The link between the command and control ground station and the UAV was designed in [35] at L- and C- bands for the Ecuadorian Air Force. In the following text, we will give preliminary tutorial on the UAV distance, link losses, link fadings and metrics.

A. UAV LINK BUDGET

Before deployment of UAVs and ground station, we should evaluate the operating distance. Considering refractive effects of atmospheric layers, the optical horizon d_o can be verified to be $d_o = \sqrt{2k_eRh}$. Under normal weather conditions $k_e = 4/3$ is to consider the four-third Earth effect, that is, the actual radio wave refraction behavior is described by an Earth with an extended radius of $4/3R$. This leads to a radio horizon $d_r \approx 4.12\sqrt{h_A}$ (h_A in m and d_r in km) [7], as shown in Fig. 3. The formula is calibrated by a statistically measured parameter by the ITU. The same distance can also be calculated using the Pythagoras' theorem without considering Fresnel and other parameters like above the sea level (asl) [36].

The free space path loss model is valid only when there is an unobstructed LOS path between the transmitter and the receiver and no objects in the first Fresnel zone. As shown in Fig. 4, the first Fresnel zone determines the minimum separation that should exist between the UAV and the highest obstacle in the path of the radio link. For a point at a given distance along the path of propagation, the radius of the first

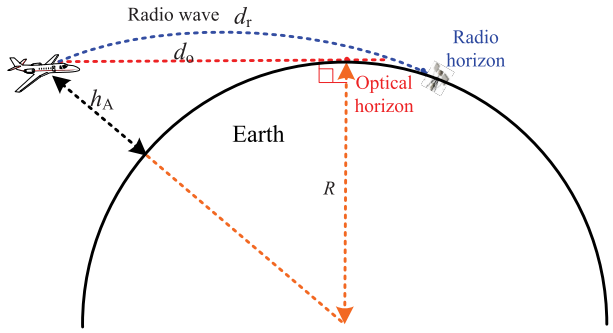

FIGURE 3. Radio horizon distance.

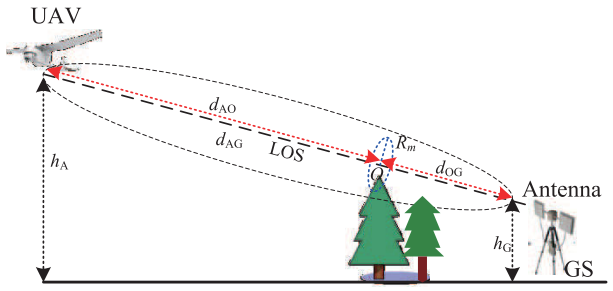

FIGURE 4. First Fresnel zone for A2G link.

Fresnel zone is given as:

$$R_m = \sqrt{\frac{\lambda d_{AO} d_{OG}}{d_{AO} + d_{OG}}}, \tag{1}$$

where d_{AO} is the distance in km of the point O from UAV, d_{OG} is the distance of the point O from ground station. For $d_{AO} = d_{AG}$, $R_m \approx 8.656\sqrt{d_{AG}/f}$. As the obstruction moves towards tangent to the LOS path, signal losses will be as much as 6 dB or more. Best practice is to maintain at least 60% of the first Fresnel zone radius free of obstructions to avoid fading of the received signal.

Without loss of generality, we exemplify the link budget method as presented in Table 1. The transmitted equivalent isotropic radiated power (EIRP) equals to sum of output power of power amplifier and antenna gain: EIRP $= G_T + P_T$. Then, the received power at receiver side is computed as,

$$P_R = G_T + P_T - L_T - L_F - L_R - L_A - L_O + G_R, \tag{2}$$

where L_F is free space loss for LOS communication link, L_R is rain attenuation loss, L_A is gaseous atmosphere loss which consists of the effects of water vapor or dry air, and L_O is other fading loss. The total losses L_T for uplink and downlink consist of receiver feeder loss, antenna off-axis loss, polarization mismatch loss, radome loss, transmitter loss, receiver pointing loss, and receiver cable loss.

- Free space loss L_F in dB is expressed as,

$$L_F = 92.45 + 20\log f + 20\log d, \tag{3}$$

where f is frequency in GHz, and d is the distance in km.

TABLE 1. Link budget table for UAV link.

Parameters	Expression	Unit
Carrier frequency	f	GHz
Bandwidth	B_N	MHz
Distance	d	km
Tx power	P_T	dBm
Tx antenna gain	G_T	dBi
Tx EIRP = G_T+P_T	EIRP	dBm
Tx feeder and cable	L_{tf}	dB
Antenna off-axis	L_{oa}	dB
Radome loss	L_{rd}	dB
Polarization mismatch	L_{pm}	dB
Pointing loss	L_{pt}	dB
Rx feeder and cable	L_{rf}	dB
Implementation loss	L_{im}	dB
Total losses	L_T	dB
Free space loss	L_F	dB
Rain attenuation	L_R	dB
Atmospheric gases	L_A	dB
Other losses	L_O	dB
Rx antenna gain	G_R	dBi
Rx power	P_R	dBm
Antenna noise	T_A	K
Rx noise	T_R	K
Thermal noise $T_N = T_A + T_R$	T_N	K
Noise figure	F_N	dB
Rx noise power	P_N	dBm
$C/N = P_R - P_N$	C/N	dB
Receiver sensitivity	P_S	dBm
Excess margin $P_m = P_R - P_S$	P_m	dB

- Rain attenuation L_R can be obtained from Recommendation ITU-R P.838 [37] and procedure described in [38]. As given typically in [39], very heavy rainfall (100 mm/h) can produce 0.4 dB/km of attenuation at 5 GHz if the rain is uniformly heavy throughout the entire signal path, which is very unlikely. For L-band, rain attenuation of 30 km distance is negligible, i.e., approximately 0.3 dB (0.01 dB/km).
- Link attenuation L_A in dB due to atmospheric gases (absorption by oxygen and water vapor) is

$$L_A = \gamma_a d, \tag{4}$$

where γ_a is the specific attenuation in dB/km, being computed for a propagation path slightly inclined, i.e., low elevation angles, assuming a temperature of 15°C, an air pressure of 1, 013 hPa and a water-vapour density of 7.5 g/m^3 for a standard atmosphere. For the two LOS bands, 1000 MHz (960 MHz – 977 MHz) and 5000 MHz (5030 MHz – 5091 MHz), γ_a equals to 5.4×10^{-3} dB/km and 7.4×10^{-3} dB/km, respectively.
- Losses L_O due to multipath, shadowing, beam spreading and scintillation can be examined by using the method of small percentages of time in [38] to compute the fading depth. This kind of signal fading will be investigated together with the path loss in next section.

At the receiver, the antenna noise temperature and Rx noise temperature are set as T_A and T_R, respectively, resulting in equivalent noise temperature $T_N = T_A + T_R$. The noise power

can be calculated as,

$$P_N = k(T_A + T_R)B_N + F_N, \tag{5}$$

where $k = -228.6$ dBW/K/Hz is Bolzmann's constant, and downlink noise figure is F_N.

Finally, we can get the carrier-to-noise power ratio as $C/N = P_R - P_N$, considering the signal fading margin L_O. The received power P_R can be compared to the receiver sensitivity P_S to evaluate the flight link margin P_m. Furthermore, for the case of amplify-and-forward (AF) relay typically in FANET, the linear C/N value received at the destination node, after two consecutive links of different C/N values: γ_1 and γ_2, should be calculated as

$$C/N = \gamma_1\gamma_2/(\gamma_1 + \gamma_2). \tag{6}$$

B. UAV CHANNEL FADING

From the link budget above, we can roughly divide the airborne communication channel characteristics into two types:

- Large-scale fading, arising from path loss of signal as a function of distance and shadowing by large objects such as buildings and hills.
- Small-scale fading, resulting from the constructive and destructive interference of the multiple signal paths between the transmitter and receiver. Multipath fading can also arise from the aircraft itself, while these are typically weak and have a very small relative delay.

Compared with mobile wireless channel, UAV air-to-ground channels will often be more dispersive, incur larger terrestrial shadowing attenuations, and change more rapidly. The channel factors include reflection, scattering, diffraction, and shadowing effects together with a direct LOS path.

- Reflection occurs when the elevation angle is low enough for the mainlobe of the receiving antenna to "see" the ground.
- Scattering is known as another type of reflection and can occur in the atmosphere or in reflections from very rough objects [40].
- Shadowing may occur due to surface-based obstacles, such as buildings, terrain, or trees but can also occur from the aircraft itself during flight maneuvers.

Reliable UAV datalinks should adapt to the associated rapidly fluctuating link quality [41]. For UAVs, we express the flight states during the maneuvering: yaw, roll, pitch, and heading, as given in Fig. 5. Some measured results in the literature are obtained under these conditions, which critically challenge the reliability of A2G or A2A links.

C. CHANNEL IMPULSE RESPONSE AND METRICS

Considering the channel fading, an LOS channel with both specular and diffuse multipath is characterized by the impulse response

$$h(t) = a_0\delta(t) + a_1 e^{j\Delta\theta_1} e^{j\Delta\omega_{d,1}(t-\tau_1)}\delta(t-\tau_1) + \xi(t)e^{j\Delta\omega_{d,2}(t-\tau_2)}\delta(t-\tau_2), \tag{7}$$

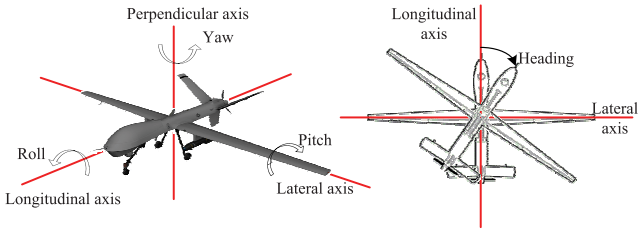

FIGURE 5. UAV flight states of pitch, yaw, roll and heading.

where a_0 and a_1 are the amplitude of the LOS signal component and the specular reflection, respectively; $\Delta\theta_1$ is the phase shift of the specular reflection relative to the LOS component; $\Delta\omega_{d,1}$ and $\Delta\omega_{d,2}$ are the Doppler shifts of the specular reflection and diffuse multipath, respectively, relative to the LOS component; τ_1 and τ_2 are the their delays relative to the LOS component; and $\xi(t)$ is a complex zero-mean Gaussian random process.

On the other hand, the time-varying complex baseband channel impulse response (CIR) [20] can be expressed generally as follows:

$$h(t,\tau) = \sum_i a_i(t)e^{-j\phi_i(t)}\delta[t - \tau_i(t)], \tag{8}$$

where a_i, ϕ_i, τ_i denote the time-varying amplitude, phase and delay of i-th multipath component (MPC), respectively.

The power ratio between the LOS and the diffuse components, the so-called Rice factor [17], is given by

$$K = \frac{a_0^2}{c^2}, \quad \text{or} \quad K_{\text{dB}} = 10\log(\frac{a_0^2}{c^2}), \tag{9}$$

where a_0^2 is the power of LOS signal, c^2 is the power of the diffuse process.

Delay dispersion modeling plays an important role in channel characterization. The delay dispersion can be characterized by three parameters namely, excess delay, the mean excess delay and root mean squared (RMS) delay spread.

- Power delay profile (PDP) characterizes the multipath fading channel giving information about channel delay, amplitude and power of individual path.
- Mean excess delay (MED) is the average of delay weighting each path by its contributing power relative to the overall power of all paths.
- RMS delay spread (RMS-DS) is a power-weighted standard deviation in delay. For the PDP of 3GPPs specified rural area channel model, the RMS delay spread equals to $\sigma_\tau = 100$ ns [7], [42].

We can quantify the delay dispersion by the RMS-DS expression as follows:

$$\sigma_\tau = \sqrt{\frac{\sum_{k=0}^{L-1} a_k^2\tau_k^2}{\sum_{k=0}^{L-1} a_k^2} - \mu_\tau^2}, \tag{10}$$

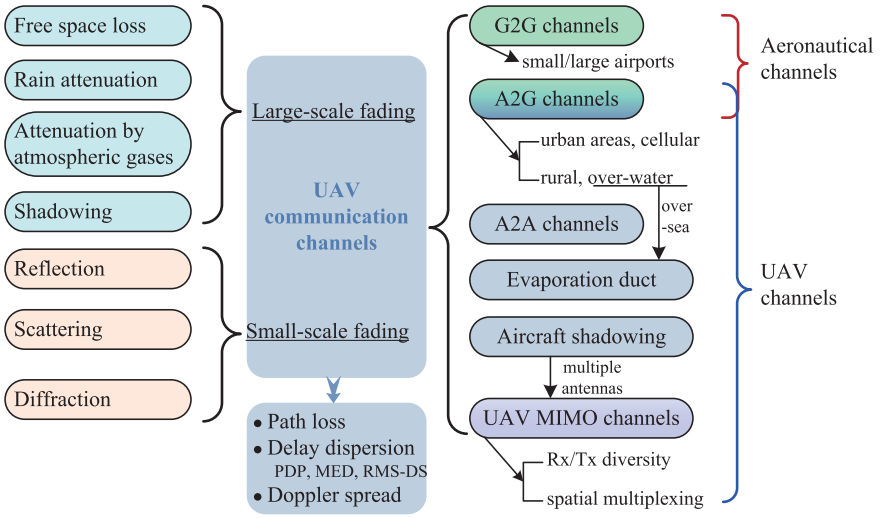

FIGURE 6. UAV communications channel classifications of scenarios.

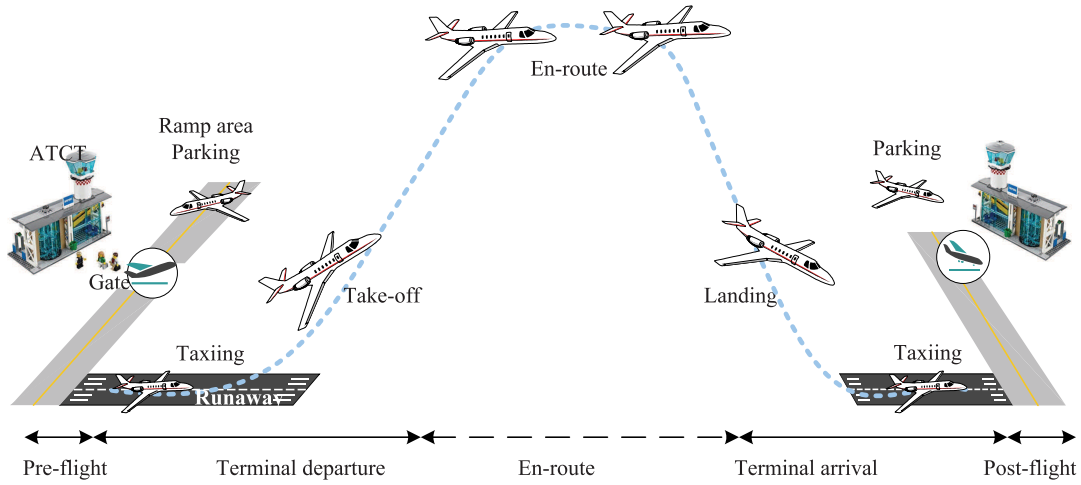

FIGURE 7. Flight phases of civil aeronautical communications.

where L denotes the number of MPCs. The mean excess delay is given by

$$\mu_\tau = \frac{\sum_{k=0}^{L-1} a_k^2 \tau_k}{\sum_{k=0}^{L-1} a_k^2}. \tag{11}$$

When either the UAV transmitter or the receiver is in high-speed motion, Doppler frequency shift is experienced by the radio signal. Doppler spread in the frequency domain is a measure of the spectral broadening caused by the time rate of change of mobile radio channel. Doppler spread is inversely proportional to the coherence time of the channel. The RMS delay spread is inversely proportional to coherence bandwidth. The details of coherence bandwidth and coherence time are explained in [40], [43].

Considering the diverse range of categories of UAVs including the aerial platforms like aircraft, airship, balloon [44], the measured results for civil aeronautical communication would be referable for designing UAV communication, especially for large unmanned aircrafts. If it is not particularly explained, we will employ "UAV channel" for UAV communication channel modeling and "aeronautical channel" for civil aeronautical communication channel modeling in the following text. To have an intuitive understanding of the UAV channels surveyed in this paper, we illustrate the channel classifications in Fig. 6 before providing detailed channel characteristics.

III. AERONAUTICAL COMMUNICATION CHANNELS

For an average assumed total duration 4 hours of all 5 phases of aircraft operation, the duration of each phase is given by ITU-R [45]: pre-flight (4%), departure (8%), en-route (76%), arrival (11%) and post-flight (1%), as shown in Fig. 7. About 85% of the spectrum demand for CNPC communication is attributed to downlink and only 15% to uplink.

TABLE 2. Typical aeronautical communication scenarios [17].

Scenario	En-Route	Arrival, Takeoff	Taxi	Parking
Link	A2G, A2A	A2G	on the ground	on the ground
Fading type	two-ray	Rician	Rician	Rayleigh
	fast fading	fast fading	slow fading	slower fading
Doppler PDF	Jakes	Jakes	Jakes	Jakes
Scattered beamwidth	3.5°	180°	360°	360°
Delay	two-ray	exponentially one-sided	exponentially	exponentially

Therefore, most of the channel measurements of civil aeronautical communication follow these scenarios and report the results of A2G and G2G links.

A. AIR-TO-GROUND AERONAUTICAL CHANNELS

The first aeronautical A2G channel characterization based on measurements during flight tests was reported in [46], where the mathematical model used link geometry and surface roughness to describe the received signal. The measurement is done at a carrier frequency of 1463 MHz and elevation angles of 0.5° – 45°. Haas [17] characterized the aeronautical channel small-area fading with statistical methods, and developed a class of aeronautical wideband channel models, featuring the parking and taxi environments, takeoff and landing situations, and en-route scenarios for both air-to-ground and air-to-air links, as shown in Table 2. Performance results depend on the underlying maximum ranges and shapes of the Doppler and delay spectra, and the presence of an LOS path. The measured results show max delay of 7μs and 33μs for parking and en-route phases, respectively. Employing wide-sense stationary uncorrelated scattering (WSSUS) channel [16], the author presents two channel emulators: flat fading and frequency-selective fading channels as expressed in (12), as shown at the bottom of this page, where the simulating orthogonal frequency division multiplexing (OFDM) system uses 128 subcarriers, each spaced 3.84 kHz at carrier frequency 5 GHz.

The similar environments of parking/taxiing, takeoff/landing and en-route were investigated in [47], where the authors modeled the A2G telemetry link in C-band at the Airbus Saint-Martin site. The ground station automatic tracking receiver antenna is a dish antenna with diameter of 2.4 m. The transmitter two small fin antennas at the aircraft nose and tail have a hemispherical transmission characteristic, and achieve transmit delay diversity. They develop TDL modeling using the sounding results of the delay, Doppler and gain of multipath components [48]. They also assume wide-sense stationarity over the short time interval and simplify the linear time-variant system (13) to be (14),

$$h(t,\tau)=\sum_{n=1}^{N}\underbrace{a_n(t,\tau)}_{\text{path gain}}\underbrace{e^{j(2\pi f_0\tau_n(t)+\theta_n(t,\tau))}}_{\text{phase}}\underbrace{\delta(\tau-\tau_n(t))}_{\text{delay}} \tag{13}$$

$$h(\tau)=\sum_{n=1}^{N}\underbrace{a_n}_{\text{path gain}}\underbrace{e^{j\theta_n}}_{\text{phase}}\underbrace{\delta(\tau-\tau_n)}_{\text{delay}} \tag{14}$$

where f_0 denotes carrier frequency, $2\pi f_0\tau_n(t)$ represents the phase shift due to free space propagation of n-th MPC under f_0, and $\theta_n(t,\tau)$ is the additive phase shift.

They arrive at conclusion as follows,

- Take-off and landing are the most time-varying flight phases with Doppler spread up to 2.5 kHz and delay spread up to 34 μs;
- Parking or slowly taxiing has multipath components with high delay spread of 20 μs;
- En-route has measured Doppler shifts in the range of −3.6 kHz to 4.1 kHz.

A two-ray aeronautical channel model simulation with OFDM signals was conducted in [36], which also followed the similar environments and modeled the LOS path with a single Doppler shift, and the reflected path with Doppler spread. We notice that these measured results of aeronautical channel are not completely consistent with each other, because of distinctive experimental waveforms, frequencies, aircrafts and environments in their measurement campaigns.

Rice *et al.* [49], [50] modeled the narrowband and wideband channels for multipath fading in aeronautical telemetry applications. The signal bandwidth in narrowband channel models is much less than the coherence bandwidth of the multipath fading process, whereas that in wideband channel models is on the order of or larger than the coherence bandwidth of the multipath fading process. They perform narrowband channel sounding tests by measuring the magnitude and phase of a single frequency from the automatic

$$h(t,\tau)=\begin{cases}\lim\limits_{N\to\infty}\dfrac{1}{\sqrt{N}}\displaystyle\sum_{n=1}^{N}\underbrace{e^{j\theta_n}}_{\text{phase}}\underbrace{e^{j2\pi f_{D_n}t}}_{\text{Doppler}}, & \text{flat fading}\\ \lim\limits_{N\to\infty}\dfrac{1}{\sqrt{N}}\displaystyle\sum_{n=1}^{N}\underbrace{e^{j\theta_n}}_{\text{phase}}\underbrace{e^{j2\pi f_{D_n}t}}_{\text{Doppler}}\underbrace{\delta(t-\tau_n)}_{\text{delay}}, & \text{frequency selective fading}\end{cases} \tag{12}$$

TABLE 3. Airport classes for channel characterization study.

Class	Building	Flight	Example airports	Serving aircrafts
Large	international airport, high ATCT (50 – 85 m), many large buildings	busy, over 80 flights per hour	John F. Kennedy International Airport, Beijing Capital International Airport	B747, B777, A380
Medium	regional and local airport, high ATCT, one main terminal building	busier than GA airports	Cleveland Hopkins International Airport, Beijing Nanyuan Airport	regional jets to larger jets B737, A320
Small	GA airport, low ATCT (10 – 15 m) or no ATCT	no scheduled service	Burke Lakefront Airport in Cleveland	single- / twin-propeller aircrafts

gain control (AGC) records and the wideband one using frequency domain analysis of 10 Mbps binary phase shift keying (BPSK) signal. Their results illustrate that,

1) for narrowband channel, it includes an LOS signal, a specular reflection strength (20% to 80% that of the LOS signal), and a diffuse multipath component, the power of which is 10 dB to 20 dB less than that of the LOS signal;
2) for wideband channel, it is composed of three propagation paths: an LOS direct path and two specular reflections. The first specular reflection caused by a specular ground ''bounce'' or reflection is characterized by a relative amplitude of 70% to 96% of the LOS amplitude and a delay of 10 ns – 80 ns. The gain of second path with a much lower amplitude and a longer delay is modeled as a zero-mean complex Gaussian random variable, with 2% to 8% of the LOS amplitude and mean excess delay of 155 ns with an RMS-DS of 74 ns.

Their transmitter adopts a linear power amplifier (output power of 2 W) and vertically polarized hemispherically omnidirectional antenna. Their receiving station uses a parabolic reflector to track the airborne transmitter. They model the channel as a TDL with time-varying coefficients to account for changes in the characteristics of the multipath. The dominant feature of the multipath interference is the spectral null generated by the first multipath reflection. They find that the multipath interference is during mission critical portions with low elevation angle for both narrowband and wideband channels.

Recently, Schneckenburger *et al.* [51] proposed a geometry-based stochastic channel model [52] for the A2G channel in a regional airport environment in the L-band based on an exhaustive propagation measurement campaign to reproduce the non-stationarity of the channel impulse response, and validated the channel model using LDACS range measurements. They conclude that their modeling approach would be very precise for roll angles below 5°. For aircraft-to-ground channels, Rieth *et al.* [53] conducted two measurement campaigns at the small airport of Ingolstadt/Manching in Germany to characterize taxiways and runways, and flight patterns in near proximity to the airport, respectively. They develop a miniaturized sounder generating complex linearly swept frequency pulses with chirp bandwidth of 42 MHz and an airborne C-band (5.121 GHz) blade antenna under H36 Dimona aircraft. Their S-band GS antenna is mounted on top of a building with an elevation of 24 m to manually and automatically track UAV using telemetry positioning data from the aircraft. Large-scale fading results for aircraft shadowing and antenna misalignment effects, and small-scale fading results for K-factors, delay and Doppler spread statistics are recorded and analyzed.

B. GROUND-TO-GROUND AERONAUTICAL CHANNELS

Matolak *et al.* [54], [55] developed the empirical stochastic channel models at both large and small airport surface environments at 5 GHz. According to the airport classes in [54], large airports refer to the busy ones at major cities designed with many large airplanes (e.g., 747s, 777s and A380) moving around throughout the day, typically 80 or more during a busy hour. They usually have terminal buildings, airline hangars, maintenance buildings, parking garages on the airport property, and many large hotels and office buildings adjacent to them. Example airports in this class are John F. Kennedy International Airport and Beijing Capital International Airport. In comparison, the medium airports (e.g., Cleveland Hopkins International Airport and Beijing Nanyuan Airport) usually have only one main terminal building, whereas they are significantly bigger and busier than small general aviation (GA) airports (e.g., Burke Lakefront airport in Cleveland). For small GA airports, we commonly see single- and twin-propeller aircrafts, smaller height of the air traffic control tower (ATCT), smaller airport surface area and link distances less than 2 km. This airport classification for the purposes of channel characterization study is summarized in Table 3.

The outdoor G2G links between an ATCT (50 m – 85 m for large airport and 10 m – 15 m for small airport) and a ground vehicle (4 km or 2 km coverage) are measured at the ''taxi'' and ''parking'' scenarios using omnidirectional monopoles antennas with 1.5 dBi gain. They classify airports link regions into three areas: LOS-Open (LOS-O), NLOS-Specular (NLOS-S), and NLOS. They develop TDL model by processing PDPs and a log-distance path loss model with exponents $n_e = 2$ to 2.3 for the LOS and NLOS-S areas,

$$L_{NLOS-S} = 103 + 10(n_e)\log(\frac{d}{d_0}) + X, \qquad (15)$$

where $d_0 = 462$ m is their reference distance, X is a zero-mean Gaussian random variable with a standard deviation of 5.3 dB for their system, and the attenuation of 103 dB is close to the free-space value. For the LOS-O areas, the path loss exponent is essentially that of free space, i.e., $n_e = 2$.

They find that there is less dispersion for the small airport channel than for the channel present at large/medium airports.

$$h(t,\tau) = \sum_{k=0}^{L(t)-1} z_k(t) a_k(t) \underbrace{e^{j[\omega_{D,k}(t)(t-\tau_k(t))-\omega_c \tau_k(t)]}}_{\text{phase}} \underbrace{\delta(\tau-\tau_k(t))}_{\text{delay}} \tag{16}$$

They get the median RMS-DS range from 500 ns to 1000 ns, whereas the 90th percentile values are very close to 1.7 μs. They also find that neighboring multipath components often exhibit correlated behavior, which makes them cannot assume the classical WSSUS environment. They provide channel models for bandwidth of 10 MHz and 5 MHz. The nonstationary CIR model utilizes tap persistence matrices to model the tap lifetime and Weibull distribution for tap amplitude. It is expressed in (16), as shown at the top of this page, where $a_k(t)$ represents the k-th resolved amplitude, $\omega_{D,k}(t)$ is Doppler shift, and $z_k(t)$ is a ''persistence process'' accounting for the finite time of propagation paths. The k-th resolved component consists of multiple terms received in the k-th delay bin, and $L(t)$ is a time-varying number of transmission paths.

Aeronautical mobile airport communications system (AeroMACS) is a derivative of the IEEE 802.16 – 2009 standard and is developed in cooperation with the WiMAX forum by Europe and the U.S. [19], [56]. For airport AeroMACS data link, Gligorevic [56] characterized the path loss and multipath fading of the airport surface channel using omnidirectional antenna with 3 dBi gain at 5.2 GHz. The dominant LOS is expected in ground and taxi areas. The most comparable to their results is the medium airport class of [54] by Matolak. The linear regression curve for path loss in the prevailing LOS ground and tower areas is given as,

$$L_{LOS} = 10(n_e)\log\frac{d}{d_0} + A(d_0), \tag{17}$$

where the resulting path loss exponent is $n_e = 2.4$ and the intercept value $A = 86.7$ dB corresponds to the free space loss at a distance of 100 m.

The simplest path loss model in ramp area is expressed as,

$$L_{NLOS} = 10(n_e)\log\frac{d}{d_0} + A(d_0) + X + L_s, \tag{18}$$

where X is zero-mean Gaussian random variable, L_s is the additional loss due to shadowing in the NLOS regions. Hence, they assume $L_s = 0$ for the ground area and $L_s = 12$ dB for NLOS ramp area.

Although the channel is in general nonstationary, the author adopts the WSSUS assumption within one AeroMACS data frame. The multipath fading characteristics is evaluated in terms of Rice factor and delay spread. The distribution of the LOS amplitude for a moving receiver has Rice factor of 11 dB. The delay spread in the NLOS ramp area is considerably higher than in the ground and tower areas. The author fits PDP curve linearly for most CIR power functions in the form $P[\text{dB}] = A + B\tau$, where A and B are regression coefficients [56].

Then, a sum-of-sinusoids based stochastic TDL model is developed with fixed randomly chosen channel parameters for the aircraft-to-tower channel. For the l-th tap, the fading process complex fading coefficient is computed as,

$$h_l(iT) = \sum_{n=0}^{N_H-1} C_{l,n}\cos(2\pi f_{l,n} iT + \varphi_{l,n}), \tag{19}$$

where N_H denotes the number of sinusoids used for generation of the fading process, the amplitudes $C_{l,n}$ are determined by power spectrum, $\varphi_{l,n}$ is a uniformly distributed random phase angle, and $f_{l,n}$ represents the Doppler frequency resolution.

For the forward link of AeroMACS with four different areas of apron, taxi, parking and runway, the most critical parking scenario were investigated in [57] based on assumption of WSSUS model. For the l-th tap, the complex fading coefficient is also generated with the sum of sinusoids method as

$$h_l(iT) = \frac{1}{\sqrt{N_H}} \sum_{n=0}^{N_H-1} C_{l,n} e^{j[(2\pi(f_{l,n}+f_l)iT)+\phi_{l,n}]}, \tag{20}$$

where the fading amplitude is given by a normalization coefficient, and f_l is Doppler frequency shift, $f_{l,n}$ is Doppler frequencies being selected according to a Gaussian power spectral density [58]. Their results show that a basic 1×2 single-input multiple-output (SIMO) scheme could enhance the diversity with maximum ratio combining (MRC).

The NLOS and LOS conditions of AeroMACS system at the taxing and parking areas of Barajas airport were studied using a linear frequency modulation (FM) chirp signal in [59], where base stations with sector antennas at heights $h_A = 12$ m, 38 m, and mobile station with an omnidirectional antenna at $h_G = 1.2$ m were used. They suggest that the pico-cells would cover the gate areas, and macro-cells would cover the rest of the airport surface.

- The LOS model is a combination of the direct ray and the ground reflected ray (21), as shown at the bottom of the next page, where $d_1 = \sqrt{d^2 + (h_A - h_G)^2}$, $d_2 = \sqrt{d^2 + (h_A + h_G)^2}$, and ρ denotes the reflection coefficient of the ground. The ground reflected ray will lead to oscillations in the path loss curves [60]. The characteristic oscillations in the path loss will occur for distances up to the cross-over distance $d_c = 4\pi h_A h_G/\lambda$ [48]. For shorter distances than d_c, the path loss exponent has $n_e = 2$, while for larger distances than d_c, n_e increases to 4.
- The NLOS is a two-slope path loss model (22), as shown at the bottom of the next page, where f is the operating frequency in GHz, d is the distance in meters and d_0

TABLE 4. Civil aeronautical channels measurements and modeling.

Literature	Frequency	Scenario	Sounding	Signal	Channel model	Aircraft
[17]	VHF, 5 GHz	A2G, A2A	PDP, Doppler PDF	OFDM	WSSUS	Boeing 747-400
[47]	5.12–5.15 GHz	A2G	PDP	OFDM	TDL	Airbus A380
[49]	2.25 / 2.2345 / 2.3455 GHz	narrowband A2G	magnitude, phase	pilot tone	LOS, specular reflection, diffuse multipath	B-2, missile, Super Hornet
[50]	1.5 / 2.2 GHz	wideband A2G	frequency domain	BPSK	LOS, two specular reflections	T-39 Saberliner
[53]	5.121 GHz	small airport	RMS-DS, Doppler, K-factor	chirp pulses	Large- and small-scale fading	H36 Dimona
[54]	5 GHz	large airport	RMS-DS, FCE, PDP	PN DS-SS	TDL	/
[55]	5 GHz	small airport	RMS-DS, FCE, PDP	PN DS-SS	TDL	/
[56]	5.2 GHz	airport surface	PDP	AeroMACS OFDM	TDL	/
[59]	5.09–5.15 GHz	airport surface	delay spread	AeroMACS	two-ray	/

is named by break point distance. The shadowing X_σ is modeled as a log-normal distributed variable for a pure NLOS channel.

The typical aeronautical channels described above for A2G and G2G links are summarized in Table 4, where some other measurements sharing similar results are not presented. We compare the measurements in the literatures in terms of scenario, sounding, signal and channel models. Most of these aeronautical channels were sounded with PDPs and modeled by TDL. From the results, we can find that the aeronautical channels vary depending on the phases of flight, and can be assumed to be WSSUS for A2G and A2A links, whereas the channels at airport tend to be nonstationary.

IV. UAV COMMUNICATION CHANNELS

A. AIR-TO-GROUND CHANNELS

1) A2G CHANNELS IN URBAN AREAS

A model-based fading statistics analysis of UAV A2G channel in an urban area was given by Simunek *et al.* [61] with low elevation angle ranging from about 1° to 6°. Their remotely controlled airship has two missions, path-loss and shadowing models, respectively. Their airborne transmitter uses continuous wave signal with power of 27 dBm and a monopole antenna at 2 GHz. It stores the global positioning system (GPS) position, pitch and roll data. A four-channel receiver for performing diversity studies is used and receiver sensitivity is −126 dBm with bandwidth of 12.5 kHz. They express the distribution of the received signal by second-order statistics, the power spectral density and the autocorrelation function, under the Rice assumption with a strong coherent component plus a diffuse contribution. They develop a narrowband time-series synthesizer containing two main blocks: one generates the diffuse component while the other one generates the direct/coherent signal. They conclude that the Loo (Rice + log-normal) model is the most suitable for the low elevation link dynamic characteristics, which lie between the purely terrestrial and the land mobile satellite channel.

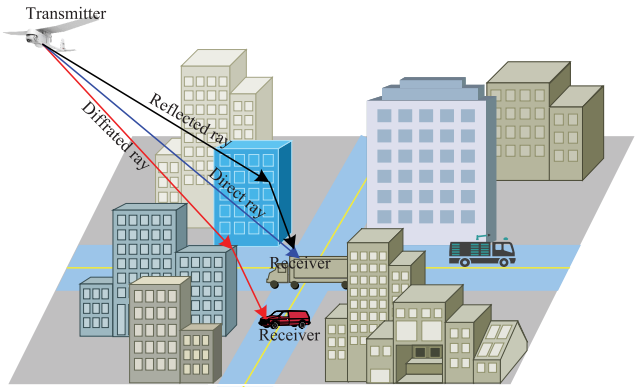

FIGURE 8. Propagation phases of UAV A2G channels [62].

The path loss and shadowing models of UAV A2G channels were investigated by Kakar [7], where the shadowing model followed the shadowing path loss study of HAP in [62] at 2.0 GHz, 3.5 GHz, and 5.5 GHz for 3G and 4G mobile systems. The path loss is described as the sum of FSL and excessive path loss. In case of NLOS, it includes two phases of propagation: from the airborne station to the first ground obstacle and from that obstacle to the ground station, as shown in Fig. 8. The path losses in LOS and

$$L_{LOS} = 20\log\left(\frac{\lambda}{4\pi}\right) + 10\log\left(\left|\frac{1}{d_1}e^{-j2\pi d_1/\lambda} + \frac{\rho}{d_2}e^{-j2\pi d_2/\lambda}\right|^2\right) \tag{21}$$

$$L_{NLOS} = \begin{cases} 32.45 + 20\log(f) + 20\log(d) + X_\sigma, & d < d_0 \\ 32.45 + 20\log(f) + 20\log(d_0) + 10(n_e)\log(\frac{d}{d_0}) + X_\sigma, & d \geq d_0 \end{cases} \tag{22}$$

$$L = \begin{cases} 32.45 + 20\log(f) + 20\log(d) + \xi_{LOS}, & \text{LOS} \\ 32.45 + 20\log(f) + 20\log(d) + L_s + \xi_{NLOS}, & \text{NLOS} \end{cases}, \quad d = \frac{\Delta h}{\sin\theta}, \tag{23}$$

NLOS scenarios can be expressed in (23), as shown at the top of this page, where d is the distance in km between airborne and ground station, L_s represents a random shadowing as a function of the elevation angle. L_s is computed using the normal distribution [62],

$$\mu_{NLOS}, \sigma_{NLOS} = \frac{g + \theta}{h + i\theta}, \tag{24}$$

where θ is the elevation angle in degrees and g, h, i are empirical parameters. Random components ξ_{LOS} and ξ_{NLOS} in dB are added as a location variability utilizing the log-normal distribution with a zero mean, whereas the standard deviation is 3 dB – 5 dB, 8 dB – 12 dB for LOS, NLOS connections, respectively.

A statistical propagation model was developed with ray tracing simulator in [63] to predict the A2G path loss from an LAP to a terrestrial terminal in urban environments. The virtual-city environment being similar to Manhattan follows the ITU-R statistical parameters at 700 MHz, 2000 MHz and 5800 MHz, with elevation angles above 15°. Their A2G path loss has LOS condition, or without LAP LOS but coverage via strong reflection and refraction. Recently, the probabilistic LAP model [63] was combined with a learning-based measurement technique to help plan the UAV relay trajectory in [64]. For ultra low altitude (0 m – 100 m) in simplified environment from Google Sketchup at Campus Sur of Technical University of Madrid, Chu *et al.* [65] conducted ray tracing simulation to analyzing A2G channels with path loss, K-factor, multipath and delay spread at 1.2 GHz and 4.2 GHz. They reveal that the multipath components experience a progress of decreasing with height ascending. To replay the measured or simulated A2G radio channels of various scenarios in lab environment in a repeatable and controlled way, Miao *et al.* [66] simulated the UAV A2G channel in low altitude by ray tracer, and emulated the simulated channel in multi-probe anechoic chamber (MPAC) using over-the-air (OTA) testing techniques [67].

2) LOW ALTITUDE CHANNELS IN CELLULAR NETWORKS

UAV communication is also gaining attention within the 3GPP standardization activities. The path loss exponents and shadowing of the channel models between UAVs and LTE cellular networks was investigated at 800 MHz in [68], where flying LTE UAV-UE (user equipment) with dipole antenna was connected to two real LTE networks in Denmark. They assess the effects of heights with distances 1 km – 22 km, elevation angles 0.25° – 2.9°, and averaged path loss samples and distances to obtain a least square regression to fit the log-distance alpha-beta (AB) model [48]. They conclude that, as the UAV moves up with higher UE heights, there are better radio clearance and decreasing path loss exponent, approximating free space propagation for horizontal ranges up to tens of kilometers and UAV heights around 100 m. This finding is corroborated by increasing interference level and number of detected interfering cells. The log-AB model is,

$$L_{AB} = \alpha 10\log(d) + \beta + X_\sigma \tag{25}$$

where d is distance in meter, α represents the path loss exponent and β is the intercept point with the line $d = 1$ m, and X_σ is a random variable that accounts for shadowing variation modeled with normal distribution and standard deviation σ.

Using ultra-low altitude (5 m – 15 m) UAVs to deliver 5G cellular mobile services, Catherwood *et al.* [69] investigated the channel gain, mean time delay and the RMS spread of the delay at three different drone heights for an open area, a tree-lined environment, and an enclosed area at 3.4 GHz – 3.8 GHz. They find that it is Rician distributed for the received signal strength, whereas mean time delay and RMS-DS for the open and tree-lined environments are Weibull distributed with the enclosed area tests being lognormally distributed. Cellular base stations (BSs) usually feature down-tilted antennas in order to reduce the co-channel interference and to confine the cell coverage area. The propagation characteristics of cellular LTE-to-UAV channel for flying altitude at 15 m – 120 m [70] are presented with the path-loss being a function of the depression angle and the terrestrial coverage beneath the UAV. They conclude that increasing depression angle will lead to a reduction in the obstacles between the UAV and the tower and thus a reduction in the path-loss, which starts to increase as the effect of down-tilted antenna pattern dominates (4° – 8°).

For low altitude A2G channel investigations, Cai *et al.* [71]–[73] investigated the path loss, shadow fading, fast fading, delay spread and Doppler frequency spread with passive channel sounding approach for different heights (15 m – 300 m) and horizontal distances (100 m – 500 m) in a suburban scenario at campus of Tongji University, Shanghai. Their air part with quasi-omnidirectional packaged discone antenna onboard the six-wing UAV receives the 18 MHz bandwidth of the LTE downlink signals with a complex sampling rate of 25 MHz at the carrier frequency of 2.585 GHz. They also present physical interpretation of the UAV channels by exploiting the propagation graph modeling approach. The channel in low heights exhibits much more MPCs, and less MPCs are observed with increasing height.

For horizontal and vertical flights, they modify the close-in log-distance free path loss models respectively as:

$$L_h = 10(n_h)\log(d) + X_h + B_h, \tag{26}$$

$$L_v = 10(n_d)\log(h) + X_d + B_d, \tag{27}$$

where path loss exponent n_h negatively correlates with height: $n_h = -0.02 \cdot h + 3.42 + n_\sigma$, the standard deviation of n_σ is calculated as 0.48, n_d is affected by both link distance positions and BS antenna pattern, X_h and X_d denote the shadow fading, and B_h and B_d represent the intercept.

- For horizontal flights, normal distribution $\mathcal{N}(0, 2.7)$ is found to best fit the empirical distribution of X_h in dB. Due to the downward BS antenna radiation pattern, Rice K-factor at the height of 15 meters is larger than that of the other heights from 30 to 100 meters, where $\mathcal{N}(12.6, 5.1)$ and $\mathcal{N}(7.6, 5.6)$ are found to best fit their empirical distributions. Similarly, $\mathcal{N}(-7.4, 0.2)$ and $\mathcal{N}(-7.1, 0.3)$ are found to best fit delay spreads in logarithm scale for these two cases of heights.
- For vertical flights, the shadow fading is similar, with $\mathcal{N}(0, 3.0)$ fitting the empirical distribution of X_d in dB. For positions $d = 100, 200$ m, and $d = 300 - 500$ m, $\mathcal{N}(15.2, 4.7)$ and $\mathcal{N}(8.4, 3.8)$ are found to fit the empirical distributions of K-factor, respectively. For positions $d = 100 - 400$ m, and $d = 500$ m, $\mathcal{N}(-6.97, 0.25)$ and $\mathcal{N}(-7.33, 0.13)$ are found to fit the delay spread empirical distributions, respectively.

Similarly, Qiu *et al.* [74] carried out vertical (0 m – 100 m) and horizontal (20 m – 100 m) flight measurements in low altitudes with continuous wave transmitter installed at the lower part of a small hexacopter UAV, providing path loss exponent at different altitudes and a height-dependent Rice K-factor model. Their two cloverleaf antennas are circularly polarized with omnidirectional radiation pattern on the horizontal plane and a 3dB beamwidth of 60° and 55° at 1200 MHz for L-band and 4200 MHz for C-band. Their ground station antenna is vertically polarized with a gain of 3 dB – 5 dB and its half-power beamwidth in elevation is 50°.

3) A2G CHANNELS IN RURAL AND OVER-WATER AREAS

Recently, Matolak *et al.* [20]–[22] modeled the UAS wideband A2G channels of CNPC links under three environments: suburban and near-urban scenarios, hilly and mountainous terrains, and over-water scenario. Their elevation angles range from 1.6° to 40°, and aircraft pitch and roll angles, and aircraft heading are recorded. The path loss, small-scale fading, spatial and inter-frequency correlations for multiple aircraft antennas, RMS-DS, and wideband TDL models are investigated. The path loss is described by either log-distance with a correction for flight direction (28), or two-ray models (29), as shown at the bottom of this page.

$$L_{\log} = A_0 + 10(n_e)\log\frac{d}{d_0} + X + \alpha F \tag{28}$$

In (28) and (29), A_0 are the constants at the minimum valid link distances d_0, F denotes the small adjustment factors for direction of travel, X are zero-mean Gaussian random variables, B_L is the average difference between the measured path loss and the CE2R (curved earth two-ray) model, φ is the grazing angle, $a(d)$ is a unit-energy Rician fading variable, and $\alpha = -1, +1$ for travel toward or away receiver, respectively. The FE2R (flat-earth two-ray) or CE2R models are path loss models considering the ground roughness influence [20].

For the first two environments, the TDL models include up to nine taps, accounting for the LOS component, a ground reflection, and up to seven MPCs, whereas the intermittent rays are termed as the third ray for the over-water environment. The equation for the complex baseband CIR for the AG channels is (30), as shown at the bottom of this page, where α, φ, τ denote the amplitude, phase, and delay, respectively, $z_k \in \{0, 1\}$ denotes the k-th MPC on/off parameter described by the occurrence probability. The first two terms are computed from the CE2R model.

They use channel stationarity distance (SD) and equal width sliding window to calculate small-scale Rice K-factor. Assuming wide-sense stationary channel, their SD is 15 m for all environments. Their measurements show that the median values of K-factor range from 12 dB to 14.7 dB for L-band and 27 dB to 30 dB for C-band in the suburban, hilly or over-water settings, which are almost independent of link range and environment due to the presence of a strong LOS component. For the aircraft flying over mountains or hills, the ground station (GS) local terrain may still be flat, hence allowing for a strong specular reflection, and scattering as well. Multiple aircraft antennas on the bottom of the aircraft provide almost no diversity gain for the A2G channels in strong LOS conditions, for the moderate values of antenna separation.

A 3-ray multipath model was employed by Lei and Rice [75] to characterize the aeronautical telemetry channel frequency responses over the Pacific Ocean. Their measurement signal of equal power tones is received by a 4 ft parabolic reflector antenna operating at 8 GHz. Their model consists of an LOS path and two reflected propagation paths. The strong specular reflection is determined by the geometry defined by the airborne transmitter, the ground-based receiver, and the sea surface. Its delay lies between 10 ns

$$L_{2ray} = \begin{cases} \mathrm{FE2R}(d) - 20\log[a(d)], & \varphi_{\min} < \varphi \\ \mathrm{CE2R}(d) + B_L + \alpha F - 20\log[a(d)], & \varphi_{\min} < \varphi < \pi/2 \end{cases} \tag{29}$$

$$h(t,\tau) = \begin{cases} a_{LOS}(t)\delta(\tau - \tau_1(t)) + a_2(t)e^{-j\varphi_2(t)}\delta(\tau - \tau_2(t)) + \sum_{k=3}^{9} z_k(t)\alpha_k(t)e^{-j\varphi_k(t)}\delta(\tau - \tau_k(t)), & \text{suburban} \\ a_{LOS}(t)\delta(\tau - \tau_1(t)) + a_2(t)e^{-j\varphi_2(t)}\delta(\tau - \tau_2(t)) + z_3(t)\alpha_3(t)e^{-j\varphi_3(t)}\delta(\tau - \tau_3(t)), & \text{over-water} \end{cases} \tag{30}$$

TABLE 5. UAV channel measurements and modeling for A2G links.

Literature	Frequency	Scenario	Sounding	Signal	Channel model	Aircraft
[61]	2 GHz	1 – 6°	path-loss, shadowing	continuous wave	Loo (Rice + log-normal)	airship
[62]	2.0/3.5/5.5 GHz	0 – 90°	shadowing	continuous wave simulation	elevation dependent channel	HAP airship
[63]	0.7/2.0/5.8 GHz	> 15°	ITU statistical parameters	ray tracing simulation	LOS, strong reflection, refraction	LAP
[68]	0.8 GHz	0.25 – 2.9°	path-loss, shadowing	LTE	log-distance alpha-beta model	commercial UAV
[71]	2.585 GHz	h: 15 – 300 m, d: 100 – 500 m	PDP, RMS-DS, Doppler	LTE downlink	close-in path loss models	six-wing UAV
[69]	3.4 – 3.8 GHz	h: 5 – 15 m	PDP, RMS-DS	5G cellular	Rician, Weibull, log-normal	commercial drone
[22]	0.97/5 GHz	1.62 – 20.54°	PDP, RMS-DS	SIMO, DS-SS	TDL: LOS, ground reflection, 7 MPCs	S-3B Viking
[21]	0.97/5 GHz	mountainous, hilly terrains	PDP, RMS-DS	SIMO, DS-SS	CE2R, TDL with 9 taps	S-3B Viking
[20]	0.97/5 GHz	over-sea / freshwater	PDP, RMS-DS	SIMO, DS-SS	CE2R, TDL 3-ray	S-3B Viking
[75]	8 GHz	rough / calm sea	geometry PDP, RMS-DS	equal power tones (100 kHz apart)	3-ray	Beachcraft C-12 airplane
[76]	5.7 GHz	0.37 – 1.83 km msl, over-sea	PDP, LMS curve fitting	spread-spectrum BPSK	FSL and 2-ray	Learjet 35A

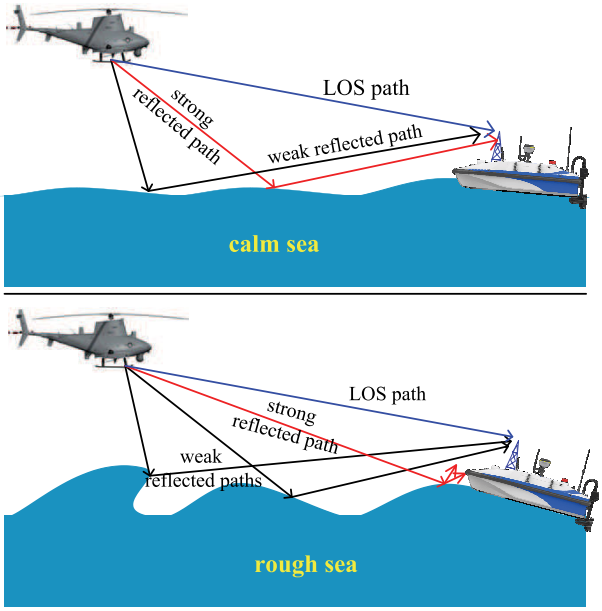

FIGURE 9. Physical interpretation of multipath propagation over calm and rough sea.

and 50 ns. For smaller random reflection, mean excess delay is 57 ns with an RMS-DS of 25 ns. They conclude that the roughness of sea water not only reduces the energy for both of these reflections but also causes these two paths to be less pronounced. For rough sea, short delay reflections contribute more to the second ray than longer delay reflections. For calm sea, the second reflection is more random and has a smaller amplitude and larger delay, as described in Fig. 9. The Rayleigh criterion is used to characterize whether a given surface is rough or not. The sea surface is considered rough only if $\sigma_r > \lambda/(8\cos\theta_i)$, where σ_r is the surface roughness, λ is the wavelength of the signal, and θ_i is the incident angle of the incoming wave. As altitude decreases, the incident angle increases, and thus, the sea surface appears to be with stronger specular reflections.

Meng and Lee [76] conducted experimental study of A2G channels at 5.7 GHz over sea surface at the South China Sea with low airborne altitudes (0.37 km – 1.83 km). Their wideband channel measurements use BPSK and spread-spectrum signals with a rate of 20 Mcps. A vertically polarized omnidirectional blade antenna is mounted on the head of an aircraft with an effective radiated power of 40 dBm. To create diversity receptor, their receiver uses two identical directional antennas with a beamwidth of 20° in azimuth and 25° in elevation. However, space diversity at the ground station may not be helpful for overcoming the signal obstruction induced by the aircraft body during aircraft maneuvering [77]. The path-loss exponents are estimated through the least mean square (LMS) curve fitting from measured data. Their measured results follow a similar trend to the predicted results from the 2-ray model.

The typical UAV channel measurements we described above for A2G links at rural and urban scenarios, and over sea or water areas are summarized in Table 5. We compare them in terms of scenario, sounding, signal and channel models. The air-to-ground links have common low elevation angle down to 1°, which will challenge the wideband communication system performance.

B. AIR-TO-AIR CHANNELS

A ray-tracing simulation for UAV A2A channel modeling at 2.4 GHz was performed in [78] over the land and over the sea with different altitudes. To model path loss, they perform simulations with fixed transmitter and circularly flying receiver with 100 m radius and 3 km distance. They derive the log-distance path loss model, and characterize the small scale

TABLE 6. UAV channels measurements for A2A links.

Literature	Frequency	Altitude	Scenario	Sounding	Signal	Channel model
[78]	2.4 GHz	500 m – 1500 m	urban, over-sea	excess delay, RMS-DS	802.11g/n, 802.16 WiMAX	log-distance path loss model, Rician fading
[80]	2.3 GHz	$<$ 1.5 km	urban, suburban, mountain, over-sea	CIR: PDPs, delay spread	20MHz OFDM	2-ray model: direct + specular diffuse path
[79]	5.06 GHz	700 m	above-ground, sea	RSS, PDPs	MSK/TDMA	LOS, multipath

fading by Rician fading. The path loss computed with the transmit-receive (Tx-Rx) distances for horizontal-horizontal (H-H) and vertical-vertical (V-V) polarizations is given as $L = a + 10(n_e)\log d$, where a refers to the Y-intercept from the least squared error fit, taking values of 77.48 dB and 63.75 dB for V-V polarization at altitude 150 m and 500 m over sea, respectively. The typical values for the K-factor lie between 10 to 15 dB for all the propagation scenarios.

To characterize delay dispersion, they consider the excess delay of the MPCs within 6 dB, 12 dB and 18 dB below the LOS component, and all the excess delayed paths arrive within 570 ns for 3 km distance and 500 m height. The RMS-DS and coherence bandwidth are compared with the OFDM guard interval and sub-carrier spacing of IEEE 802.11g/n and 802.16 WiMAX, i.e., 312.5 kHz and 10.94 kHz, respectively. Their results show that the sub-carrier spacing of WiMAX systems is smaller than the coherence bandwidth, while 802.11g/n systems exhibit frequency selective fading for its sub-carriers. The Doppler shift differs for each MPC and depends on the direction of movement, and will affect the carrier spacing or the symbol duration. Therefore, for WiMAX system, the possible synchronization errors will result in inter-carrier interference (ICI) due to its large symbol duration.

The A2A channel between fixed-wing small UAVs at C-band 5110 MHz was modeled in [79] above both ground and sea in Japan. The on-board transceiver uses time division duplexing (TDD) TDMA minimum shift keying (MSK) signal with 7 MHz bandwidth, the transmit power is 30 dBm, and the receiver sensitivity is around -95 dBm. Their vertical polarization dipole antennas have gains of 2.14 dBi. They use received signal strength (RSS) and PDP to evaluate the channels of en-route. Their channel consists of the LOS and multipath components. The first delay wave above the sea is clearer than above the ground. The maximum incoming path-delay time above the ground at an altitude less than 700 m is within 4 μs. They also characterized the A2A channel at S-band 2.3 GHz with altitude lower than 1.5 km in Hawaii [80], where the measurements used the same type of antenna, but examined 5 types ground conditions: urban, suburban, trees, mountains, and over sea areas. They use OFDM signal with 20 MHz bandwidth, subcarriers spacing of 3.8147 kHz, symbol duration of 262.1 μs, and guard interval of 32.8 μs. Transmit power at antenna terminal is 20 dBm, and receiver sensitivity is -84 dBm. They calculate CIR using IFFT and then get PDPs by averaging CIRs. They reveal that ground reflection gives an impact on the CIR for over the sea, but not for over urban areas due to obstacle of tall buildings. The diffuse components spread over 40 μs in every ground type while the case of over-the-sea is less than 10 μs.

The cooperative relay-based UAVs network over generalized fading channels were studied in [81]. Results show that Rayleigh fading is suitable for low altitude crowded area, while Nakagami-m and Weibull fading with high fading parameters fit well for high altitude open space. The measurements of an IEEE 802.11 link at 2.4 GHz in [82] extended the Rice channel model to account for multipath effects introduced by the flight altitude of UAVs. The research in [83] analyzed the bit error ratio (BER) performance of UAV communication system 802.11a OFDM signals at 5 GHz. The A2A channel is characterized to have a large Doppler shift due to high speed of the UAVs, short coherence time and large ICI. Their results show that there is a 2 dB loss for OFDM over a frequency selective Rayleigh fading channel.

The typical UAV A2A channel measurements at S- and C-bands for various scenarios we reviewed above are summarized in Table 6. Their results of channel models and path delay will be helpful in designing link budget, transmission techniques and system parameters of airborne A2A communications, especially for UAV FANETs.

C. EVAPORATION DUCT FOR OVER-SEA

The considerations of ducting and atmospheric gas attenuation were not accounted for in Matolak's work [20], [84], while the measurements in [76], [85] were reported with average elevated duct height of more than 1 km, and occurrence probability of more than 10% of the time. The FSL and 2-ray models are then found to overestimate the propagation loss. The air immediately adjacent to the ocean is saturated with water vapor. When there is a temperature increase or rapid decrease in vapor pressure, the evaporation or surface ducts arise and enhance propagation for very low-altitude UAS flights over the sea [86]. The height at which the refractivity gradient equaling zero is defined as the evaporation duct height. Evaporation duct and elevated duct over the sea surface are the two important factors that can significantly affect the over-water A2G communication link, as described in Fig. 10. Therefore, the UAV communication with low altitude flight should take ducting into account during the system design and application mission.

Meng and Lee [76], [87] also investigated possible evaporation duct and elevated duct over the sea surface and its transmission enhancement effect. The airborne transmitter

TABLE 7. Evaporation duct works comparison.

Literature	Scenario	Frequency	Enhancement	Duct heights	Site
[88]	Tx 8.5 m, Rx 10.5 m, length 27.7 km	3 – 94 GHz	50% time > 16 dB, (10.5/16 GHz)	67% time: 1–12 m	Lorient France
[89]	Tx 4.8m, 4.5 m; Rx: 19.2m, 17.8 m	0.6 – 18 GHz	20 – 30 dB (7 – 18 GHz)	0 – 40 m	Aegean Sea, North Sea
[90]	10 m	8 GHz	influence is negligible as wind speed < 5 m/s	10 m, 20 m, 30 m	simulation
[76], [87]	Tx: 0.37 – 1.83 km	5.7 GHz	50% time > 8 dB	10% time: 0.9 – 1 km	South China Sea

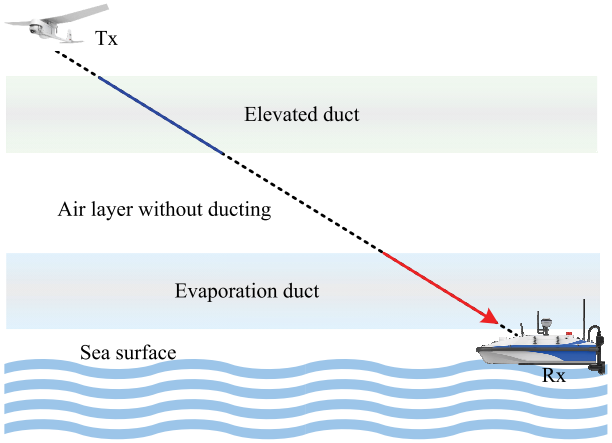

FIGURE 10. Evaporation duct and elevated duct over the sea surface.

heights are 0.37 km – 1.83 km, and receiver heights are 2.10 m and 7.65 m. They find that, as the airborne altitude decreases to 0.37 km, there is a huge increase (more than ten times) in the estimated RMS-DS, due to the significant evaporation ducting effect, which results in multi-reflections with longer propagation paths. Evaporation duct above the sea surface can lead to a substantial increase in the RSS at frequencies above 3 GHz, and their results show more than 8 dB for 50% of the propagation time at 5.7 GHz and less than 5 dB for around 15% of the time. They find that the distance-dependence of the ducting induced enhancement P_E in dB is linearly modeled, and the physical variations of the ducting layers are found to be Gaussian distributed,

$$P_E = A \times d + P_{do}, \tag{31}$$

where A is ducting coefficients on the order of 0.1 dB/km, d is distance in km, and P_{do} is empirical distance-offset signal enhancement. They also find that the sea-wind-driven roughened sea surface would reduce the specular sea-surface reflection in a ducting environment.

Without flight with UAV, the early measurement in [88] conducted the experiment at seven frequency points from 3 GHz to 94 GHz to investigate the influence of evaporation duct. The transmitter heights are 8.5 m above average tide, and the receiver heights 10.5 m. Transmission path over sea has a length of 27.7 km. They observe that duct heights range from 1 m to 12 m during more than 67% of the time, and duct height from 12 m – 15 m during 7% of the time. No ducting conditions exist for a high percentage of time (24%). The 10.5 GHz and 16 GHz signals have experienced the largest enhancement: more than 16 dB during 50% of the time. At 3 GHz, the enhancement factor is larger than 5 dB during 50% of the time. Enhancements larger than 10 dB are observed at 3 GHz, 5.6 GHz, 10.5 GHz, 16 GHz, 35 GHz and 94 GHz for 19%, 48%, 70%, 70%, 50% and 21% of the time, respectively.

The over-the-horizon propagation path loss from 0.6 GHz to 18 GHz was measured in [89] based only on long-term meteorological measurements in the Aegean Sea and North Sea area. They install transmitters at 4.5 m or 4.8 m above mean sea level (msl), and receivers at from 17.8 m to 19.2 m above msl. The path is 35.2 km in length and entirely over water. They give the accumulated frequency distributions of path loss by combining annual frequency distributions of evaporation duct height with the waveguide path-loss versus duct-height results. Their results show that evaporation duct is the dominant over-the-horizon propagation mechanism at frequencies above 2 GHz, and a net gain of 20 dB – 30 dB or more will be observed at 7 GHz – 18 GHz.

The influence of sea surface roughness on the propagation in the duct environment were studied at 8 GHz in [90]. The authors use a Gaussian antenna pattern in experiment, and assume horizontal polarization with elevation angle 0° and the beamwidth 1°. They model propagation by the parabolic equation method. The roughness of the sea surface is computed by modifying the smooth surface Fresnel reflection coefficient by a roughness parameter. Their experiments show that, in the evaporation duct environment, relative errors between smooth sea surface and rough sea surface enlarge with the increment of sea wind speeds, operating frequencies and evaporation duct height.

Communications over maritime environment have propagation problems that are substantially different from those arising in the land environment. We present the summarized measurements and simulations for evaporation duct in Table 7. For this kind of elevation angle approximating 0° over the sea, the UAS CNPC links at ITU C-band (5030 MHz – 5091 MHz) may fall into the ducting environment, especially for the UAV-aided networking.

D. AIRCRAFT SHADOWING

Wing shadowing occurs while the aircraft makes a "U-turn", in which the LOS link will be blocked by a wing during a large roll angle, as given in Fig. 5. Severe shadowing could

cause a total loss in link synchronization and connection. Airframe shadowing characteristics are independent of the local ground conditions and link distance. The shorter wavelength can be blocked and reflected by the metallic aircraft body easily. C-band signal has a significantly shorter wavelength (e.g. 0.06 m at 5 GHz) as compared to very high frequency (VHF) signal (e.g. 2.4 m at 125 MHz).

At elevation angles between 1.4° and 2.9°, the UAS LOS signal can be easily obstructed by the airplane itself, for which Sun *et al.* [91] gave results of shadowing depth, duration, multiple antenna diversity gain, and small scale fading with a medium-sized aircraft. They model shadowing loss as a function of aircraft roll angle, but it is essentially uncorrelated with shadowing duration. Median measured shadowing loss is on average 15.5 dB in C-band and 10.8 dB in L-band. Meng and Lee [92] also conducted experimental study of the shadowing effect induced by aircraft body during maneuvering for A2G communication at C-band 5.7 GHz. They carry out linear flight route and circular flight route with aircraft orientation recorded. A vertically polarized, omnidirectional blade antenna is mounted on an aircraft and two receivers with identical directional antennas are placed separately at the ground station. Their results show that, for linear flight route with roll and pitch orientations, the original LOS link can be shadowed up to 9.5 dB by the aircraft tail or wings with slight maneuvering. Transmitted signal undergoes significant shadowing attenuation up to 28 dB with forced turning maneuvering, at an altitude of 3.2 km, link distance from 35 km to 46 km. Channel measurements at 5.12 GHz for a large aircraft flying were conducted in [93] at an altitude of 11 km over a distance exceeding 100 km. They mount the antenna on the fuselage and observe the impact of the aircraft structure on the LOS path. They simulate this shadowing and find a shadowing attenuation up to 15 dB, which fits well with empirical data.

The measurements of above shadowing work share the similar results. The airframe shadowing is reported to be the primary shadowing mechanism for short to medium-range A2G links. The spatial diversity at the ground station is unable to eliminate this shadowing effect caused by the aircraft during maneuvering. Deployment of multiple airborne antennas is shown helpful to mitigate this shadowing and ensure a clear communication path for all flight scenarios. Multiple aircraft antennas can provide significant diversity gain up to 16 dB in the shadowing area, and the diversity gain is typically less than 5 dB or 6 dB outside the shadowing region [91]. The space time codes are suggested to overcome this array antennas interference, whereas spatial modulation can improve the spectral efficiency [94], [95].

V. UAV CHANNELS FOR MIMO COMMUNICATION

In this section, we will commence with the UAV MIMO channel modeling and measurement works in the literature, and then review the receive diversity, spatial multiplexing and transmit diversity (STC) techniques used in UAVs.

A. UAV MIMO CHANNELS

Zeng *et al.* [96] investigated the geometry-based stochastic model [97] used for UAV MIMO channel modeling. They investigate the space-time correlation function (STCF) under a 3D moving and scattering environment. They take only NLOS components into account in this model, and give the CIR expression between antenna elements in typical 2×2 channel. They find that for higher elevation angle, larger distance, there will be a higher temporal correlation, and they conclude that the UAV should move horizontally for reliable MIMO performance. This work was then extend to the non-stationary propagation environment and multi-hop UAV-based relay system [98]–[102].

Yanmaz *et al.* [103] investigated an 802.11a-based A2G channels using small quadrotor UAV with two on-board antennas. The transceiver uses 2×2 omnidirectional rubber antennas, with gains of 5 dBi and vertical polarization. They illustrate the impact of two different antenna orientations on the received signal strength and conclude that proper antenna orientations need to be determined for both the UAVs and ground stations before deployment.

Rice and Jensen [104] conducted experimental studies of channel near the flight-line using an airborne array with four different small blade transmit antennas at L-band 1.8 GHz. The two receive tracking antennas pointing to the GPS coordinates of the aircraft possibly results in reduced overall power but richer multipath observations. Rich multipath environment supports gains in signal-to-noise ratio (SNR) of approximately 13 dB for the two 3×1 antennas scenarios.

Newhall and Reed [105] presented an A2G channel model based on a 3D ellipsoidal geometry for airborne station in a cluttered environment. Their analysis results show that scatters are distributed in a ground region as a function of elevation angle and maximum normalized multipath delay. Then, they measure an SIMO system in [106] at 2.05 GHz for elevation angles 7.5° – 30°. A ground-based four-element monopole linear antenna array with element separation of $\lambda/2$ is used to enable receiver diversity gain. Results show that mean excess delay spread increases with decreasing elevation angle, while the number of measured multipath components tends to remain constant with elevation angles. MRC achieves diversity gains of 2.5 dB. A space-time two-dimensional rake receiver using four antenna array elements and four rake fingers per antenna element can achieve a gain of up to 7 dB.

The UAV channel with multiple antennas and their measurements are given in Table 8, designing with different configurations elaborately, 2×2, 1×4 or 3×1, and achieving rich gains for various scenarios.

B. RX/TX ANTENNA DIVERSITY

Simunek *et al.* [107] tested the low elevation link channel in [61] using a four-channel receiver, i.e. 1×4 SIMO at 2GHz. They verify the incremental C/N gains by increasing the number of diversity, at elevation angle from about

TABLE 8. UAV A2G link channel for MIMO transmission.

Literature	Antennas	Frequency	Signal	MIMO channel	Altitude
[105], [106]	vertical polarized monopulse antennas 1×4	2.05 GHz	DS-SS	MRC: diversity gains of 2.5 dB, rake receiver: 7 dB at 7.5°	1500 – 3200 feet msl
[103]	vertical polarized omnidirectional antennas 2×2	2.4/5 GHz	802.11a	H antenna - yaw, V antenna - tilting	20 – 120 m
[104]	3 blade antennas × 1 dish antenna	1800 MHz	unmodulated tones	SNR of 13 dB for rich multipath	15 – 20 feet
[96]	uniform linear array antenna	3 GHz	/	move horizontally and straight towards ground user	distance d = 100 m

1° to 4° in urban areas. Three usual combining strategies are also assessed: selection, equal-gain, and maximal ratio. The largest increment is achieved when introducing the first diversity branch. Further branches bring about smaller improvements, but still substantial. The space diversity plus combining gain is found to be practically independent of the elevation angle. Kung *et al.* [108] carried out an SIMO (1×4) low-altitude UAV G2A link measurements using 802.11b/g radios at 800 MHz. The combined packet delivery rates can be improved with gain of roughly 25% by 4 receivers. Periodically choosing the active one of multiple ground transmitters can achieve additional 12% selection diversity gain.

Willink *et al.* [109] investigated the UAV low-altitude A2G channel with two transmit antennas at 915 MHz. They mount the quarter-wave helical antennas below the UAV's wings with one wavelength from the fuselage center. A linear array of helical antennas is mounted on the roof of a van, spaced at one-half wavelengths. Two eight-channel receivers are outside and inside the flight loop respectively. The outside-loop receiver elevation angles are in the range of 13° – 21°. The inside-loop receiver maximum Doppler shift and change rates are nearly 110 Hz and 18 Hz/s, respectively. Received signals are recorded at each of eight antenna elements. Their results show that spatial diversity of outside-loop receivers is lower than inside-loop due to the close spatial similarity. There are near-field scattering at both the ground and UAV, which can be exploited to increase the capacity gains.

For frequency selective multipath channel [110], Williams [111] utilized spatial diversity with multiple receive antennas along with error-based best source selection to improve telemetry link reliability. Their transmitter antenna is omnidirectional and the ground-based large parabolic antenna is mechanically steered to track the aircraft and maximize the receiver SNR. They find that, a best source selection procedure with 2 antennas can improve BER performance up to 10 dB over the unequalized channel.

Palat *et al.* [112] applied the idea of distributed transmit beamforming and distributed orthogonal space time block coding (STBC) to cooperative UAV-assisted two-hop relay communication. Their simulation results show that distributed transmit beamforming performs better than distributed orthogonal STBC, whereas it requires accurate position information and uniformly separated UAVs. The carrier frequencies at VHF or lower may be practical depending on the dimensions of a UAV. The distributed orthogonal STBC will derive higher diversity gain with higher number of UAVs at rich multipath environment, and it is robust to position errors.

Jensen *et al.* [77] examined unitary space-time codes with multiple antennas mounted on UAV, separating by multiple wavelengths, to surmount the signal obstruction during UAV maneuvering. They conclude that Alamouti dual-antenna transmission satisfies both full diversity and angle-independent conditions. They also present that good code must maintain a strong link when the signal from one of the antennas is obstructed, and remove self-interference from multiple signals. For low elevation angle, Rice *et al.* [113] addressed the problem of multipath mitigation for shaped-offset QPSK (SOQPSK) by equalization and diversity with multiple transmit antennas. In frequency-selective fading, given the size, weight and power (SWaP) constraints, time-reversed space-time block codes (TR-STBCs) [114], [115] is a viable approach, after which the data blocks from different transmit antennas are orthogonal in the frequency domain.

Gao *et al.* [116] studied the UAV-MIMO communication system adopting 4 transmitting antennas with circular array layout on the UAV and 2 receiving antennas in the ground station. They simulate the UAV-MIMO channel capacity with different pitch, roll, yaw angles, distance and antenna array diameter. Their results show that, the larger diameter of circular antenna array leads to reduced relativity of communication channel. For larger distance, the stronger spatial correlation and hence the lower average channel capacity is observed.

C. SPATIAL MULTIPLEXING

Chen *et al.* [117] gave an analysis of 4×4 MIMO-OFDM performance for airborne wireless communication systems at 2.4 GHz. Their air platform Cessna-172S connects to several ground nodes and mount four 3 dBi omnidirectional antennas. Ground stations use directional patch antennas at rooftop with gains of 6 dBi and 1 m or 8 m separation, or omnidirectional whip antenna at airport with gains of 3 dBi and 1 m separation. Their results show that MIMO can achieve a significant gain in throughput and link range, or large Tx power savings as compared to an SISO (single-input single-output) system. At large distances with signal multipath, spatial decorrelating the received signals will allow spatial multiplexing to become more effective.

The interelement space of the interpolated MIMO antenna array based on two orthogonal linear antenna arrays [118]

can adapt to the attitude and the relative position of the aircraft to GS, hence can enlarge the capacity of the MIMO transmission. The optimal interelement space depends on the relative position to the GS [119], and a virtual antenna is constructed from a uniform linear antenna array (ULA) with the interpolation algorithm [120].

VI. CHALLENGES AND OPEN ISSUES

Equipped with diverse communication payloads, UAVs cooperating with relays and base stations constitute a space-air-ground heterogeneous network [121], [122]. UAV communication channels play a critical role in designing UAV datalink system and protocols for the heterogeneous network. In this section, we will discuss some research challenges and open issues for characterizing UAV channels.

A. ANTENNAS FOR UAV CHANNEL MEASUREMENT

The antennas are critical to enhance receiving signals quality and extend UAV coverage, especially for low elevation angle datalink at long distance [123]. Single antennas and antenna arrays have been used for sending the data back to the ground station for analysis and decision making. The antennas are designed either to be very lightweight and thin or to have part of the vehicle structure providing physical support for the antennas and electromagnetic functionality.

Generally, the antennas have omnidirectional antennas or directional antenna. Directional antenna usually require node location information for beam pointing. Small UASs with highly mobility and limited payload space requires lightweight, low-profile, conformal and lower cost omni-directional antennas for A2G and A2A communications. Relatively large UAS may also use directional highly focused beams to achieve connectivity with more distinct systems. MIMO and massive MIMO (mMIMO) techniques are a proven technology used in commercial cellular wireless systems [124]–[126]. Zhang *et al.* employ low-resolution analog-to-digital converters (ADCs) [127] and digital-to-analog converters (DACs) [128] to reduce the power consumption and hardware cost for practical mMIMO systems. The drone-based multiple antenna beamforming system can improve throughput significantly from both LOS and NLOS in-field measurements for L-, S- and C- bands [129]. While much 5G focus has gravitated towards the 60 GHz band, 5G cellular services will be delivered across a number of bands [130], [131]. The fluctuating two-ray (FTR) fading channels [132], [133] were reported to provide a much better fit than other fading models for small-scale fading measurements in millimeter wave communications [134], [135]. The multiple antenna communication and higher frequency application trends will challenge development of radio-frequency components and thus the UAV channel modeling or performance evaluation under various scenarios [136], [137].

B. CHANNELS OF UAV APPLICATIONS IN IOT AND 5G

The popularity of the Internet of things (IoT) has triggered a surge in the number of mobile data traffic for upcoming 5G and Beyond 5G (B5G) wireless networks [138], [139]. UAV will play an important role in the IoT vision, which aims at enabling things to be connected anytime, anywhere ideally using any network and providing any service [140]. UAV can be considered important IoT device or airborne UE in 5G for enhanced mobile broadband (eMBB), massive machine-type communication (mMTC) and ultra reliable low latency communication (uRLLC) scenarios. A drone manages its own sensor information for stabilization and motion planning, where synchronization among different drones is achieved via a central unit. The extremely high reliability, the low latency and jitter, opens the possibility to off-load the motion planning tasks to the cloud which can then be directly coordinated by a cloud control system [141]. The 5G based approach is scalable from a resource perspective, to a larger number of drones with only very limited computational abilities, compared with state-of-the art approaches where each drone requires a costly processor [142]. Furthermore, UAV communication networks along with traditional satellite and ground cellular networks construct a space-air-ground heterogeneous network and provide the seamless coverage as well as of improving the capacity for increasingly prosperous IoT networks [121]. These emerging applications of UAV communication in the context of IoT require channel modeling with cellular signals received from base stations.

C. CHANNELS IN VERTICAL INDUSTRIAL APPLICATIONS

Most of the research activities in the literature are related to high altitude A2G channels with large UAVs. In many rescue missions outdoor and indoor [143], the UAV application for environment sensing also requires a comprehensive modeling of the propagation channel. Zeng *et al.* applied UAV-aided AF relay in high-speed train (HST) communications to enforce railway safety and support high traffic over generalized κ-μ fading channels in [144], where the statistical SNR characteristics of the simultaneous wireless information and power transfer (SWIPT) system were derived with the random direction mobility model. Accommodating to model the UAV propagation or satellite relay link [145] in LOS scenarios, the κ-μ distribution is a general fading channel including the Rician, Nakagami-m, and Rayleigh distributions as special cases [146]. The wireless powered UAV-aided relay systems were then investigated in [147] over κ-μ fading channels providing the analytical expressions for the outage probability, the symbol error rate, and the average capacity.

Kachroo *et al.* [148] evaluated the distance and frequency dependent path loss factors for different bandwidths between a UAV and a human subject with wearable antenna under indoor warehouse environment. They reveal that log-normal distribution is the best fit distribution to model their fading statistics. Determining the communication channels among a fleet of UAVs is essential to realize future industrial IoT ecosystem [149], [150]. The A2G channels observed in various vertical applications, like UAV-aided industrial Internet [149], vehicular Internet [151] and indoor communication scenarios [148], have not been studied thoroughly.

D. CHANNELS OF UAV FSO COMMUNICATIONS

The enormous growth in IoT, and Internet video streaming from UAV networking is driving toward magnitudes of higher data rates that can be easily and sustainably achieved via Free-space optical (FSO) communication [152]. Optical routers will be more practical for unmanned high-flying vehicles like the Global Hawk, Boeing's Phantom Eye, and the X-37B. Applications could apply to fixed locations and in air-to-air scenarios. The defense advanced research projects agency (DARPA) completed the FSO Experimental Network Experiment program [153], which employed a hybrid optical/RF communication technology and demonstrated A2A and A2G point-to-point communications. To achieve average communication performance, the transmitter and receiver arrays required for current state-of-the-art commercial UAVs are problematic for such small vehicles [154]. In addition, there is a stringent LOS requirement between the transmitter and the receiver. Establishing channel models for aerial FSO links will be an important topic of future research.

VII. CONCLUSION

In this paper, we have comprehensively surveyed and analyzed the A2G, G2G and A2A channel measurements and models for both civil aeronautical communications and UAV communications. Explicitly, with the analysis of link budget of the UAV communications, we present the design guideline for managing the link budget taking account of propagation losses and link fadings. We review the channel modeling and measurements in the literature for aeronautical communications from the aspects of A2G and G2G channels under various scenarios. Then, we overview the UAV communication channels for A2G and A2A links, evaporation duct and aircraft shadowing. The channels for UAVs MIMO communications are also reviewed along with analysis of receive/transmit diversity gain and spatial multiplexing gain achieved by multiple-antenna-aided UAV communications. As reported, there are still many open issues to the design of an aerial communications for various applications. We expect that this survey would spur more research, experiments and implementations in these areas.

REFERENCES

[1] L. Gupta, R. Jain, and G. Vaszkun, "Survey of important issues in UAV communication networks," *IEEE Commun. Surv. Tuts.*, vol. 18, no. 2, pp. 1123–1152, 2nd Quart., 2015.
[2] E. C. Tetila, B. B. Machado, D. A. Guimarães, and H. Pistori, "Identification of soybean foliar diseases using unmanned aerial vehicle images," *IEEE Geosci. Remote Sens. Lett.*, vol. 14, no. 12, pp. 2190–2194, Dec. 2017.
[3] M. Khan, K. Heurtefeux, A. Mohamed, K. A. Harras, and M. M. Hassan, "Mobile target coverage and tracking on drone-be-gone UAV cyber-physical testbed," *IEEE Syst. J.*, vol. 12, no. 4, pp. 3485–3496, Dec. 2018.
[4] S. Chen, D. F. Laefer, and E. Mangina, "State of technology review of civilian UAVs," *Recent Patents Eng.*, vol. 10, no. 3, pp. 160–174, 2016.
[5] C. Yan, J. Wang, L. Fu, C. Jiang, M. Chen, and Y. Ren, "Timing synchronization and ranging in networked UAV-aided OFDM systems," *J. Commun. Inf. Netw.*, vol. 3, no. 4, pp. 45–54, 2018.
[6] J. Liu, Y. Shi, Z. M. Fadlullah, and N. Kato, "Space-air-ground integrated network: A survey," *IEEE Commun. Surveys Tuts.*, vol. 20, no. 4, pp. 2714–2741, 4th Quart., 2018.
[7] J. A. Kakar, "UAV communications: Spectral requirements, MAV and SUAV channel modeling, OFDM waveform parameters, performance and spectrum management," M.S. thesis, Virginia Polytech. Inst. State Univ., Blacksburg, VA, USA, 2015.
[8] R. E. Weibel, "Safety considerations for operation of different classes of unmanned aerial vehicles in the national airspace system," M.S. thesis, Massachusetts Inst. Technol., Cambridge, MA, USA, 2005.
[9] J. A. Volpe, "Unmanned aircraft system (UAS) service demand 2015–2035," U.S. Dept. Transp., Washington, DC, USA, Tech. Rep. DOT-VNTSC-DoD-13-01, 2014.
[10] K. Namuduri, S. Chaumette, J. H. Kim, and J. P. Sterbenz, *UAV Networks and Communications*. Cambridge, U.K.: Cambridge Univ. Press, 2018.
[11] J.-J. Wang, C.-X. Jiang, Z. Han, Y. Ren, R. G. Maunder, and L. Hanzo, "Taking drones to the next level: Cooperative distributed unmanned-aerial-vehicular networks for small and mini drones," *IEEE Veh. Technol. Mag.*, vol. 12, no. 3, pp. 73–82, Sep. 2017.
[12] E. Atkins, A. Ollero, and A. Tsourdos, *Unmanned Aircraft Systems: UAVS Design, Development and Deployment*. Hoboken, NJ, USA: Wiley, 2016.
[13] C. Guettier, P. Séchaud, J. Yelloz, G. Allard, I. Lefebvre, P. Peteuil, P. Ponthoreau, F. Cuisinier, and J. Martinet, "Improving tactical capabilities with netcentric systems: The Phoenix'08 experimentation," in *Proc. IEEE Mil. Commun. Conf. (MILCOM)*, Oct. 2009, pp. 1–7.
[14] D. H. Lyon, "A military perspective on small unmanned aerial vehicles," *IEEE Instrum. Meas. Mag.*, vol. 7, no. 3, pp. 27–31, Sep. 2004.
[15] J. Zhang, T. Chen, S. Zhong, J. Wang, W. Zhang, X. Zuo, R. G. Maunder, and L. Hanzo, "Aeronautical *ad hoc* networking for the Internet-above-the-clouds," *Proc. IEEE*, vol. 107, no. 5, pp. 868–911, May 2019.
[16] P. Bello, "Aeronautical channel characterization," *IEEE Trans. Commun.*, vol. COM-21, no. 5, pp. 548–563, May 1973.
[17] E. Haas, "Aeronautical channel modeling," *IEEE Trans. Veh. Technol.*, vol. 51, no. 2, pp. 254–264, Mar. 2002.
[18] R. Jain and F. Templin, "Requirements, challenges and analysis of alternatives for wireless datalinks for unmanned aircraft systems," *IEEE J. Sel. Areas Commun.*, vol. 30, no. 5, pp. 852–860, Jun. 2012.
[19] G. Bartoli, R. Fantacci, and D. Marabissi, "AeroMACS: A new perspective for mobile airport communications and services," *IEEE Wireless Commun.*, vol. 20, no. 6, pp. 44–50, Dec. 2013.
[20] D. W. Matolak and R. Sun, "Air–ground channel characterization for unmanned aircraft systems—Part I: Methods, measurements, and models for over-water settings," *IEEE Trans. Veh. Technol.*, vol. 66, no. 1, pp. 26–44, Jan. 2017.
[21] R. Sun and D. W. Matolak, "Air–ground channel characterization for unmanned aircraft systems—Part II: Hilly and mountainous settings," *IEEE Trans. Veh. Technol.*, vol. 66, no. 3, pp. 1913–1925, Mar. 2017.
[22] D. W. Matolak and R. Sun, "Air-ground channel characterization for unmanned aircraft systems—Part III: The suburban and near-urban environments," *IEEE Trans. Veh. Technol.*, vol. 66, no. 8, pp. 6607–6618, Aug. 2017.
[23] D. W. Matolak, "Air-ground channels & models: Comprehensive review and considerations for unmanned aircraft systems," in *Proc. IEEE Aerosp. Conf.*, Mar. 2012, pp. 1–17.
[24] J. Elston, E. W. Frew, D. Lawrence, P. Gray, and B. Argrow, "Net-centric communication and control for a heterogeneous unmanned aircraft system," *J. Intell. Robot. Syst.*, vol. 56, nos. 1–2, pp. 199–232, 2009.
[25] T. Brown, B. Argrow, C. Dixon, S. Doshi, R.-G. Thekkekunnel, and D. Henkel, "Ad hoc UAV ground network (AUGNet)," in *Proc. AIAA 3rd Unmanned Unlimited Tech. Conf.*, 2004, pp. 1–11.
[26] I. Bekmezci, O. K. Sahingoz, and Ş. Temel, "Flying ad-hoc networks (FANETs): A survey," *Ad Hoc Netw.*, vol. 11, no. 3, pp. 1254–1270, 2013.
[27] A. A. Khuwaja, Y. Chen, N. Zhao, M.-S. Alouini, and P. Dobbins, "A survey of channel modeling for UAV communications," *IEEE Commun. Surveys Tuts.*, vol. 20, no. 4, pp. 2804–2821, 4th Quart., 2018.
[28] W. Khawaja, I. Guvenc, D. W. Matolak, U.-C. Fiebig, and N. Schneckenberger, "A survey of air-to-ground propagation channel modeling for unmanned aerial vehicles," *IEEE Commun. Surveys Tuts.*, to be published.
[29] *Interaction Channel for Satellite Distribution Systems; Guidelines for the use of EN 301 790 in Mobile Scenarios*, document ETSI-TR 102 768, 2009.
[30] R. J. Kerczewski, J. D. Wilson, and W. D. Bishop, "UAS CNPC satellite link performance—Sharing spectrum with terrestrial systems," in *Proc. IEEE Aerosp. Conf.*, Mar. 2016, pp. 1–9.

[31] P. Luo, Y. Cui, and R. Li, "Novel multiband/broadband horizontally polarized omnidirectional antennas," in *Proc. IEEE Int. Symp. Antennas Propag. (APSURSI)*, Jun./Jul. 2016, pp. 1795–1796.

[32] M. S. Sharawi, D. N. Aloi, and O. A. Rawashdeh, "Design and implementation of embedded printed antenna arrays in small UAV wing structures," *IEEE Trans. Antennas Propag.*, vol. 58, no. 8, pp. 2531–2538, Aug. 2010.

[33] F. Pinkney, D. Hampel, S. DiPierro, B. S. Abbe, and M. Sheha, "UAV communications payload development," in *Proc. IEEE Mil. Commun. Conf. (MILCOM)*, Nov. 1997, pp. 403–407.

[34] H.-C. Lee, "Ku-band link budget analysis of UAV with atmospheric losses," in *Proc. IEEE/AIAA 25th Digit. Avionics Syst. Conf.*, Oct. 2006, pp. 1–8.

[35] W. Medina-Pazmiño, A. Jara-Olmedo, and D. Valencia-Redrován, "Analysis and determination of minimum requirements for a data link communication system for unmanned aerial vehicles—UAV's," in *Proc. IEEE Ecuador Tech. Chapters Meeting (ETCM)*, Oct. 2016, pp. 1–6.

[36] J. Haque, "An OFDM based aeronautical communication system," M.S. thesis, Univ. South Florida, Tampa, FL, USA, 2011.

[37] *Specific Attenuation Model for Rain for use in Prediction Methods*, document Rec. ITU-R P.838-3, 2005.

[38] *Propagation Data and Prediction Methods Required for the Design of Terrestrial Line-of-Sight Systems*, Standard ITU-R P.530, 2015.

[39] J. D. Parsons, *The Mobile Radio Propagation Channel*. Hoboken, NJ, USA: Wiley, 2000.

[40] D. Tse and P. Viswanath, *Fundamentals of Wireless Communication*. Cambridge, U.K.: Cambridge Univ. Press, 2005.

[41] J. Xie, Y. Wan, J. H. Kim, S. Fu, and K. Namuduri, "A survey and analysis of mobility models for airborne networks," *IEEE Commun. Surveys Tuts.*, vol. 16, no. 3, pp. 1221–1238, 3rd Quart., 2014.

[42] *Universal Mobile Telecommunications System (UMTS); Deployment Aspects*, document 3GPP TR 25.943, 2004.

[43] Y. S. Cho, J. Kim, W. Y. Yang, and C. G. Kang, *MIMO-OFDM Wireless Communications with MATLAB*. Hoboken, NJ, USA: Wiley, 2010.

[44] H. Shakhatreh, A. H. Sawalmeh, A. Al-Fuqaha, Z. Dou, E. Almaita, I. Khalil, N. S. Othman, A. Khreishah, and M. Guizani, "Unmanned aerial vehicles (UAVs): A survey on civil applications and key research challenges," *IEEE Access*, vol. 7, pp. 48572–48634, 2019.

[45] *Characteristics of Unmanned Aircraft Systems and Spectrum Requirements to Support Their Safe Operation in Non-Segregated Airspace*, Standard ITU-R REPORT M.2171, 2009.

[46] J. Painter, S. Gupta, and L. Wilson, "Multipath modeling for aeronautical communications," *IEEE Trans. Commun.*, vol. COM-21, no. 5, pp. 658–662, May 1973.

[47] C. Bluemm, C. Heller, B. Fourestie, and R. Weigel, "Wideband aeronautical channel sounding and modeling for C-band telemetry," in *Proc. IEEE 24th Int. Symp. Pers. Indoor Mobile Radio Commun. (PIMRC)*, Sep. 2013, pp. 264–269.

[48] T. S. Rappaport, *Wireless Communications: Principles and Practice*. Upper Saddle River, NJ, USA: Prentice-Hall, 1996.

[49] M. Rice, R. Dye, and K. Welling, "Narrowband channel model for aeronautical telemetry," *IEEE Trans. Aerosp. Electron. Syst.*, vol. 36, no. 4, pp. 1371–1376, Oct. 2000.

[50] M. Rice, A. Davis, and C. Bettweiser, "Wideband channel model for aeronautical telemetry," *IEEE Trans. Aerosp. Electron. Syst.*, vol. 40, no. 1, pp. 57–69, Jan. 2004.

[51] N. Schneckenburger, T. Jost, M. Walter, G. del Galdo, D. W. Matolak, and U.-C. Fiebig, "Wideband air–ground channel model for a regional airport environment," *IEEE Trans. Veh. Technol.*, vol. 68, no. 7, pp. 6243–6256, Jul. 2019.

[52] A. F. Molisch, A. Kuchar, J. Laurila, K. Hugl, and R. Schmalenberger, "Geometry-based directional model for mobile radio channels—Principles and implementation," *Eur. Trans. Telecommun.*, vol. 14, no. 4, pp. 351–359, 2003.

[53] D. Rieth, C. Heller, and G. Ascheid, "Aircraft to ground-station C-band channel—Small airport scenario," *IEEE Trans. Veh. Technol.*, vol. 68, no. 5, pp. 4306–4315, May 2019.

[54] D. W. Matolak, I. Sen, and W. Xiong, "The 5-GHz airport surface area channel—Part I: Measurement and modeling results for large airports," *IEEE Trans. Veh. Technol.*, vol. 57, no. 4, pp. 2014–2026, Jul. 2008.

[55] I. Sen and D. W. Matolak, "The 5-GHz airport surface area channel—Part II: Measurement and modeling results for small airports," *IEEE Trans. Veh. Technol.*, vol. 57, no. 4, pp. 2027–2035, Jul. 2008.

[56] S. Gligorevic, "Airport surface propagation channel in the C-band: Measurements and modeling," *IEEE Trans. Antennas Propag.*, vol. 61, no. 9, pp. 4792–4802, Sep. 2013.

[57] P. Pulini, "Forward link performance analysis for the future IEEE 802.16-based airport data link," in *Proc. IEEE Int. Conf. Commun.(ICC)*, May 2010, pp. 1–5.

[58] P. Hoeher, "A statistical discrete-time model for the WSSUS multipath channel," *IEEE Trans. Veh. Technol.*, vol. 41, no. 4, pp. 461–468, Nov. 1992.

[59] J. E. Hakegard, V. Ringset, and T. A. Myrvoll, "Empirical path loss models for C-band airport surface communications," *IEEE Trans. Antennas Propag.*, vol. 60, no. 7, pp. 3424–3431, Jul. 2012.

[60] A. Goldsmith, *Wireless Communications*. Cambridge, U.K.: Cambridge Univ. Press, 2005.

[61] M. Simunek, F. P. Fontán, and P. Pechac, "The UAV low elevation propagation channel in urban areas: Statistical analysis and time-series generator," *IEEE Trans. Antennas Propag.*, vol. 61, no. 7, pp. 3850–3858, Jul. 2013.

[62] J. Holis and P. Pechac, "Elevation dependent shadowing model for mobile communications via high altitude platforms in built-up areas," *IEEE Trans. Antennas Propag.*, vol. 56, no. 4, pp. 1078–1084, Apr. 2008.

[63] A. Al-Hourani, S. Kandeepan, and A. Jamalipour, "Modeling air-to-ground path loss for low altitude platforms in urban environments," in *Proc. IEEE Globecom Workshops (GC Wkshps)*, Dec. 2014, pp. 2898–2904.

[64] P. Ladosz, H. Oh, G. Zheng, and W.-H. Chen, "A hybrid approach of learning and model-based channel prediction for communication relay UAVs in dynamic urban environments," *IEEE Robot. Autom. Lett.*, vol. 4, no. 3, pp. 2370–2377, Jul. 2019.

[65] X. Chu, C. Briso, D. He, X. Yin, and J. Dou, "Channel modeling for low-altitude UAV in suburban environments based on ray tracer," in *Proc. 12th Eur. Conf. Antennas Propag. (EuCAP)*, Apr. 2018, pp. 1–5.

[66] Y. Miao, W. Fan, J. Rodríguez-Piñeiro, X. Yin, and Y. Gong, "Emulating UAV air-to-ground radio channel in multi-probe anechoic chamber," in *Proc. IEEE Globecom Workshops (GC Wkshps)*, Dec. 2018, pp. 1–7.

[67] Y. Ji, W. Fan, G. F. Pedersen, and X. Wu, "On channel emulation methods in multiprobe anechoic chamber setups for over-the-air testing," *IEEE Trans. Veh. Technol.*, vol. 67, no. 8, pp. 6740–6751, Aug. 2018.

[68] R. Amorim, H. Nguyen, P. Mogensen, I. Z. Kovács, J. Wigard, and T. B. Sørensen, "Radio channel modeling for UAV communication over cellular networks," *IEEE Wireless Commun. Lett.*, vol. 6, no. 4, pp. 514–517, Aug. 2017.

[69] P. A. Catherwood, B. Black, E. B. Mohamed, A. A. Cheema, J. Rafferty, and J. A. D. Mclaughlin, "Radio channel characterization of mid-band 5G service delivery for ultra-low altitude aerial base stations," *IEEE Access*, vol. 7, pp. 8283–8299, 2019.

[70] A. Al-Hourani and K. Gomez, "Modeling cellular-to-UAV path-loss for suburban environments," *IEEE Wireless Commun. Lett.*, vol. 7, no. 1, pp. 82–85,

[71] X. Cai, J. Rodríguez-Piñeiro, X. Yin, N. Wang, B. Ai, G. F. Pedersen, and A. P. Yuste, "An empirical air-to-ground channel model based on passive measurements in LTE," *IEEE Trans. Veh. Technol.*, vol. 68, no. 2, pp. 1140–1154, Feb. 2019.

[72] X. Cai, N. Wang, J. Rodríguez-Piñeiro, X. Yin, A. P. Yuste, W. Fan, G. Zhang, G. F. Pedersen, and L. Tian, "Low altitude air-to-ground channel characterization in LTE network," in *Proc. 13th Eur. Conf. Antennas Propag. (EuCAP)*, Mar./Apr. 2019, pp. 1–5.

[73] X. Ye, X. Cai, X. Yin, J. Rodríguez-Piñeiro, L. Tian, and J. Dou, "Air-to-ground big-data-assisted channel modeling based on passive sounding in LTE networks," in *Proc. IEEE Globecom Workshops (GC Wkshps)*, Dec. 2017, pp. 1–6.

[74] Z. Qiu, X. Chu, C. Calvo-Ramirez, C. Briso, and X. Yin, "Low altitude UAV air-to-ground channel measurement and modeling in semi-urban environments," *Wireless Commun. Mobile Comput.*, vol. 2017, pp. 1–11, Oct. 2017, Art. no. 1587412.

[75] Q. Lei and M. Rice, "Multipath channel model for over-water aeronautical telemetry," *IEEE Trans. Aerosp. Electron. Syst.*, vol. 45, no. 2, pp. 735–742, Apr. 2009.

[76] Y. S. Meng and Y. H. Lee, "Measurements and characterizations of air-to-ground channel over sea surface at C-band with low airborne altitudes," *IEEE Trans. Veh. Technol.*, vol. 60, no. 4, pp. 1943–1948, May 2011.

[77] M. A. Jensen, M. D. Rice, and A. L. Anderson, "Aeronautical telemetry using multiple-antenna transmitters," *IEEE Trans. Aerosp. Electron. Syst.*, vol. 43, no. 1, pp. 262–272, Jan. 2007.

[78] S. N. Venkatasubramanian, "Propagation channel model between unmanned aerial vehicles for emergency communications," M.S. thesis, Aalto Univ., Helsinki, Finland, 2013.
[79] F. Ono, T. Kagawa, H. Tsuji, R. Miura, and F. Kojima, "Measurements on C-band air-to-air channel for coexistence among multiple unmanned aircraft systems," in *Proc. Int. Conf. Unmanned Aircr. Syst. (ICUAS)*, Jun. 2017, pp. 1160–1164.
[80] K. Takizawa, F. Ono, M. Suzuki, H. Tsuji, and R. Miura, "Measurement on S-band radio propagation characteristics for unmanned aircraft systems," in *Proc. 8th Eur. Conf. Antennas Propag. (EuCAP)*, Apr. 2014, pp. 3068–3072.
[81] I. Y. Abualhaol and M. M. Matalgah, "Performance analysis of cooperative multi-carrier relay-based UAV networks over generalized fading channels," *Int. J. Commun. Syst.*, vol. 24, no. 8, pp. 1049–1064, 2011.
[82] N. Goddemeier and C. Wietfeld, "Investigation of air-to-air channel characteristics and a UAV specific extension to the Rice model," in *Proc. IEEE Globecom Workshops (GC Wkshps)*, Dec. 2015, pp. 1–5.
[83] Z. Wu, H. Kumar, and A. Davari, "Performance evaluation of OFDM transmission in UAV wireless communication," in *Proc. 37th Southeastern Symp. Syst. Theory*, Mar. 2005, pp. 6–10.
[84] D. W. Matolak and R. Sun, "Unmanned aircraft systems: Air-ground channel characterization for future applications," *IEEE Veh. Technol. Mag.*, vol. 10, no. 2, pp. 79–85, Jun. 2015.
[85] Y. H. Lee and Y. S. Meng, "Analysis of ducting effects on air-to-ground propagation channel over sea surface at C-band," in *Proc. Asia–Pacific Microw. Conf. Proc. (APMC)*, Dec. 2011, pp. 1678–1681.
[86] S. P. A. Balkees, K. Sasidhar, and S. Rao, "A survey based analysis of propagation models over the sea," in *Proc. Int. Conf. Adv. Comput., Commun. Inform. (ICACCI)*, Aug. 2015, pp. 69–75.
[87] Y. H. Lee and Y. S. Meng, "Empirical modeling of ducting effects on a mobile microwave link over a sea surface," *Radio Eng.*, vol. 21, no. 4, pp. 1054–1059, 2012.
[88] H. J. M. Heemskerk and R. B. Boekema, "The influence of evaporation duct on the propagation of electromagnetic waves low above the sea surface at 3-94 GHz," in *Proc. 8th Int. Conf. Antennas Propag.*, Mar./Apr. 1993, pp. 348–351.
[89] H. V. Hitney and R. Vieth, "Statistical assessment of evaporation duct propagation," *IEEE Trans. Antennas Propag.*, vol. 38, no. 6, pp. 794–799, Jun. 1990.
[90] X. Zhao, S. Huang, and H. Fan, "Influence of sea surface roughness on the electromagnetic wave propagation in the duct environment," in *Proc. 2nd IITA Int. Conf. Geosci. Remote Sens. (IITA-GRS)*, Aug. 2010, pp. 467–470.
[91] R. Sun, D. W. Matolak, and W. Rayess, "Air-ground channel characterization for unmanned aircraft systems—Part IV: Airframe shadowing," *IEEE Trans. Veh. Technol.*, vol. 66, no. 9, pp. 7643–7652, Sep. 2017.
[92] Y. S. Meng and Y. H. Lee, "Study of shadowing effect by aircraft maneuvering for air-to-ground communication," *AEU-Int. J. Electron. Commun.*, vol. 66, no. 1, pp. 7–11, 2012.
[93] J. Kunisch, I. de la Torre, A. Winkelmann, M. Eube, and T. Fuss, "Wideband time-variant air-to-ground radio channel measurements at 5 GHz," in *Proc. 5th Eur. Conf. Antennas Propag. (EUCAP)*, Apr. 2011, pp. 1386–1390.
[94] B. Raddadi, N. Thomas, C. Poulliat, and M.-L. Boucheret, "On the use of spatial modulation in aeronautical communications," in *Proc. IEEE 12th Int. Conf. Wireless Mobile Comput., Netw. Commun. (WiMob)*, Oct. 2016, pp. 1–8.
[95] C. Xu, T. Bai, J. Zhang, R. Rajashekar, R. G. Maunder, Z. Wang, and L. Hanzo, "Adaptive coherent/non-coherent spatial modulation aided unmanned aircraft systems," *IEEE Wireless Commun.*, to be published.
[96] L. Zeng, X. Cheng, C.-X. Wang, and X. Yin, "A 3D geometry-based stochastic channel model for UAV-MIMO channels," in *Proc. IEEE Wireless Commun. Netw. Conf. (WCNC)*, Mar. 2017, pp. 1–5.
[97] X. Yin and X. Cheng, *Propagation Channel Characterization, Parameter Estimation, and Modeling for Wireless Communications*. Hoboken, NJ, USA: Wiley, 2016.
[98] Q. Zhu, K. Jiang, X. Chen, W. Zhong, and Y. Yang, "A novel 3D non-stationary UAV-MIMO channel model and its statistical properties," *China Commun.*, vol. 15, no. 12, pp. 147–158, Dec. 2018.
[99] X. Chen, X. Hu, Q. Zhu, W. Zhong, and B. Chen, "Channel modeling and performance analysis for UAV relay systems," *China Commun.*, vol. 15, no. 12, pp. 89–97, Dec. 2018.
[100] H. Jiang, Z. Zhang, and G. Gui, "Three-dimensional non-stationary wideband geometry-based UAV channel model for A2G communication environments," *IEEE Access*, vol. 7, pp. 26116–26122, 2019.
[101] H. Jiang, Z. Zhang, L. Wu, and J. Dang, "Three-dimensional geometry-based UAV-MIMO channel modeling for A2G communication environments," *IEEE Commun. Lett.*, vol. 22, no. 7, pp. 1438–1441, Jul. 2018.
[102] R. Jia, Y. Li, X. Cheng, and B. Ai, "3D geometry-based UAV-MIMO channel modeling and simulation," *China Commun.*, vol. 15, no. 12, pp. 64–74, Dec. 2018.
[103] E. Yanmaz, R. Kuschnig, and C. Bettstetter, "Channel measurements over 802.11a-based UAV-to-ground links," in *Proc. IEEE Globecom Workshops (GC Wkshps)*, Dec. 2011, pp. 1280–1284.
[104] M. Rice and M. Jensen, "Multipath propagation for helicopter-to-ground MIMO links," in *Proc. IEEE Military Commun. Conf. (MILCOM)*, Nov. 2011, pp. 447–452.
[105] W. G. Newhall and J. H. Reed, "A geometric air-to-ground radio channel model," in *Proc. IEEE Military Commun. Conf. (MILCOM)*, Oct. 2002, pp. 632–636.
[106] W. G. Newhall, R. Mostafa, C. Dietrich, C. R. Anderson, K. Dietze, G. Joshi, and J. H. Reed, "Wideband air-to-ground radio channel measurements using an antenna array at 2 GHz for low-altitude operations," in *Proc. IEEE Mil. Commun. Conf. (MILCOM)*, Oct. 2003, pp. 1422–1427.
[107] M. Simunek, F. P. Fontan, P. Pechac, and F. J. D. Otero, "Space diversity gain in urban area low elevation links for surveillance applications," *IEEE Trans. Antennas Propag.*, vol. 61, no. 12, pp. 6255–6260, Dec. 2013.
[108] H. T. Kung, C.-K. Lin, T.-H. Lin, S. J. Tarsa, and D. Vlah, "Measuring diversity on a low-altitude UAV in a ground-to-air wireless 802.11 mesh network," in *Proc. IEEE Globecom Workshops (GC Wkshps)*, Dec. 2010, pp. 1799–1804.
[109] T. J. Willink, C. C. Squires, G. W. K. Colman, and M. T. Muccio, "Measurement and characterization of low-altitude air-to-ground MIMO channels," *IEEE Trans. Veh. Technol.*, vol. 65, no. 4, pp. 2637–2648, Apr. 2016.
[110] *Telemetry Standards*, IRIG Standard 106-17, Telemetry Group, Range Commanders Council, 2017.
[111] I. E. Williams, "Multipath mitigation for aeronautical telemetry with multiple antennas," in *Proc. Int. Telemetering Conf.*, 2009, pp. 1–11.
[112] R. C. Palat, A. Annamalau, and J. R. Reed, "Cooperative relaying for ad-hoc ground networks using swarm UAVs," in *Proc. IEEE Military Commun. Conf. (MILCOM)*, Oct. 2005, pp. 1588–1594.
[113] M. Rice, M. S. Afran, and M. Saquib, "Equalization in aeronautical telemetry using multiple transmit antennas," *IEEE Trans. Aerosp. Electron. Syst.*, vol. 51, no. 3, pp. 2148–2165, Jul. 2015.
[114] E. Lindskog and A. Paulraj, "A transmit diversity scheme for channels with intersymbol interference," in *Proc. IEEE Int. Conf. Commun. (ICC)*, Jun. 2000, pp. 307–311.
[115] Y. Zhu and K. B. Letaief, "Single-carrier frequency-domain equalization with decision-feedback processing for time-reversal space-time block-coded systems," *IEEE Trans. Commun.*, vol. 53, no. 7, pp. 1127–1131, Jul. 2005.
[116] X. Gao, Z. Chen, and Y. Hu, "Analysis of unmanned aerial vehicle MIMO channel capacity based on aircraft attitude," *WSEAS Trans. Inf. Sci. Appl.*, vol. 10, no. 2, pp. 58–67, Feb. 2013.
[117] J. Chen, B. Daneshrad, and W. Zhu, "MIMO performance evaluation for airborne wireless communication systems," in *Proc. IEEE Mil. Commun. Conf. (MILCOM)*, Nov. 2011, pp. 1827–1832.
[118] C. Zhang, K. Pang, and L. Ma, "Interpolated airborne MIMO antenna array," *IEEE Antennas Wireless Propag. Lett.*, vol. 14, pp. 72–75, 2015.
[119] B. Holter, J. E. Hakegard, and T. A. Myrvoll, "On the use of MIMO in aeronautical communications," in *Proc. ENRI Int. Workshop ATM/CNS*, 2010, pp. 1–22.
[120] C. Zhang and K. Pang, "Two-dimensional circle antenna layout for aeronautical MIMO communications," *IEEE Antennas Wireless Propag. Lett.*, vol. 12, pp. 1566–1569, 2013.
[121] J. Wang, C. Jiang, Z. Wei, C. Pan, H. Zhang, and Y. Ren, "Joint UAV hovering altitude and power control for space-air-ground IoT networks," *IEEE Internet Things J.*, vol. 6, no. 2, pp. 1741–1753, Apr. 2019.
[122] B. Li, Z. Fei, Z. Chu, F. Zhou, K.-K. Wong, and P. Xiao, "Robust chance-constrained secure transmission for cognitive satellite–terrestrial networks," *IEEE Trans. Veh. Technol.*, vol. 67, no. 5, pp. 4208–4219, May 2018.

[123] J. Zhang, S. Chen, R. G. Maunder, R. Zhang, and L. Hanzo, "Adaptive coding and modulation for large-scale antenna array-based aeronautical communications in the presence of co-channel interference," *IEEE Trans. Wireless Commun.*, vol. 17, no. 2, pp. 1343–1357, Feb. 2018.

[124] P. Chandhar, D. Danev, and E. Larsson, "Massive MIMO for communications with drone swarms," *IEEE Trans. Wireless Commun.*, vol. 17, no. 3, pp. 1604–1629, Mar. 2018.

[125] G. Geraci, A. Garcia-Rodriguez, L. G. Giordano, D. López-Pérez, and E. Björnson, "Understanding UAV cellular communications: From existing networks to massive MIMO," *IEEE Access*, vol. 6, pp. 67853–67865, 2018.

[126] J. Zhang, B. Zhang, S. Chen, X. Mu, M. El-Hajjar, and L. Hanzo, "Pilot contamination elimination for large-scale multiple-antenna aided OFDM systems," *IEEE J. Sel. Topics Signal Process.*, vol. 8, no. 5, pp. 759–772, Oct. 2014.

[127] J. Zhang, L. Dai, Z. He, S. Jin, and X. Li, "Performance analysis of mixed-ADC massive MIMO systems over Rician fading channels," *IEEE J. Sel. Areas Commun.*, vol. 35, no. 6, pp. 1327–1338, Jun. 2017.

[128] J. Zhang, L. Dai, Z. He, B. Ai, and O. A. Dobre, "Mixed-ADC/DAC multipair massive MIMO relaying systems: Performance analysis and power optimization," *IEEE Trans. Commun.*, vol. 67, no. 1, pp. 140–153, Jan. 2019.

[129] Y. Shi, R. Enami, J. Wensowitch, and J. Camp, "Measurement-based characterization of LOS and NLOS drone-to-ground channels," in *Proc. IEEE Wireless Commun. Netw. Conf. (WCNC)*, Apr. 2018, pp. 1–6.

[130] J. Zhang, S. Chen, R. G. Maunder, R. Zhang, and L. Hanzo, "Regularized zero-forcing precoding-aided adaptive coding and modulation for large-scale antenna array-based air-to-air communications," *IEEE J. Sel. Areas Commun.*, vol. 36, no. 9, pp. 2087–2103, Sep. 2018.

[131] J. Zhang, S. Chen, X. Guo, J. Shi, and L. Hanzo, "Boosting fronthaul capacity: Global optimization of power sharing for centralized radio access network," *IEEE Trans. Veh. Technol.*, vol. 68, no. 2, pp. 1916–1929, Feb. 2019.

[132] J. Zheng, J. Zhang, S. Chen, H. Zhao, and B. Ai, "Wireless powered UAV relay communications over fluctuating two-ray fading channels," *Phys. Commun.*, vol. 35, Aug. 2019, Art. no. 100724.

[133] J. Zheng, J. Zhang, G. Pan, J. Cheng, and B. Ai, "Sum of squared fluctuating two-ray random variables with wireless applications," *IEEE Trans. Veh. Technol.*, to be published.

[134] J. Zhang, W. Zeng, X. Li, Q. Sun, and K. P. Peppas, "New results on the fluctuating two-ray model with arbitrary fading parameters and its applications," *IEEE Trans. Veh. Technol.*, vol. 67, no. 3, pp. 2766–2770, Mar. 2018.

[135] W. Zeng, J. Zhang, S. Chen, K. P. Peppas, and B. Ai, "Physical layer security over fluctuating two-ray fading channels," *IEEE Trans. Veh. Technol.*, vol. 67, no. 9, pp. 8949–8953, Sep. 2018.

[136] S. Chen, J. Zhang, G. K. Karagiannidis, and B. Ai, "Effective rate of MISO systems over Fisher–Snedecor $\mathcal{F}$ fading channels," *IEEE Commun. Lett.*, vol. 22, no. 12, pp. 2619–2622, Dec. 2018.

[137] J. Zhang, L. Dai, S. Sun, and Z. Wang, "On the spectral efficiency of massive MIMO systems with low-resolution ADCs," *IEEE Commun. Lett.*, vol. 20, no. 5, pp. 842–845, Feb. 2016.

[138] B. Li, Z. Fei, and Y. Zhang, "UAV communications for 5G and beyond: Recent advances and future trends," *IEEE Internet Things J.*, vol. 6, no. 2, pp. 2241–2263, Apr. 2019.

[139] B. Li, Z. Fei, Y. Zhang, and M. Guizani, "Secure UAV communication networks over 5G," *IEEE Wireless Commun.*, to be published.

[140] N. H. Motlagh, T. Taleb, and O. Arouk, "Low-altitude unmanned aerial vehicles-based Internet of Things services: Comprehensive survey and future perspectives," *IEEE Internet Things J.*, vol. 3, no. 6, pp. 899–922, Dec. 2016.

[141] J. Wang, C. Jiang, Z. Ni, S. Guan, S. Yu, and Y. Ren, "Reliability of cloud controlled multi-UAV systems for on-demand services," in *Proc. IEEE Global Commun. Conf.*, Dec. 2017, pp. 1–6.

[142] I. T. Monroy, T. R. Raddo, S. Rommel, C. Okonkwo, N. Calabretta, U. Johannsen, G. Dubbelman, J. Scholtes, and B. Rutten, "Testing facilities for end-to-end test of vertical applications enabled by 5G networks: Eindhoven 5G Brainport testbed," in *Proc. 20th Int. Conf. Transparent Opt. Netw. (ICTON)*, Jul. 2018, pp. 1–5.

[143] S. Hayat, E. Yanmaz, and R. Muzaffar, "Survey on unmanned aerial vehicle networks for civil applications: A communications viewpoint," *IEEE Commun. Surveys Tuts.*, vol. 18, no. 4, pp. 2624–2661, 4th Quart., 2016.

[144] W. Zeng, J. Zhang, K. P. Peppas, B. Ar, and Z. Zhong, "UAV-aided wireless information and power transmission for high-speed train communications," in *Proc. 21st Int. Conf. Intell. Transp. Syst. (ITSC)*, Nov. 2018, pp. 3409–3414.

[145] W. Zeng, J. Zhang, D. W. K. Ng, B. Ai, and Z. Zhong, "Two-way hybrid terrestrial-satellite relaying systems: Performance analysis and relay selection," *IEEE Trans. Veh. Technol.*, vol. 68, no. 7, pp. 7011–7023, Jul. 2019.

[146] J. Zhang, X. Chen, K. P. Peppas, X. Li, and Y. Liu, "On high-order capacity statistics of spectrum aggregation systems over κ-μ and κ-μ shadowed fading channels," *IEEE Trans. Commun.*, vol. 65, no. 2, pp. 935–944, Feb. 2017.

[147] S. Chen, J. Zhang, W. Zeng, K. P. Peppas, and B. Ai, "Performance analysis of wireless powered UAV relaying systems over κ-μ fading channels," in *Proc. IEEE Globecom Workshops (GC Wkshps)*, Dec. 2018, pp. 1–6.

[148] A. Kachroo, S. Vishwakarma, J. N. Dixon, H. Abuella, A. Popuri, Q. H. Abbasi, C. F. Bunting, J. D. Jacob, and S. Ekin, "Unmanned aerial vehicle-to-wearables (UAV2W) indoor radio propagation channel measurements and modeling," *IEEE Access*, vol. 7, pp. 73741–73750, 2019.

[149] Z. Zhou, C. Zhang, C. Xu, F. Xiong, Y. Zhang, and T. Umer, "Energy-efficient industrial Internet of UAVs for power line inspection in smart grid," *IEEE Trans. Ind. Informat.*, vol. 14, no. 6, pp. 2705–2714, Jun. 2018.

[150] M. Gharibi, R. Boutaba, and S. L. Waslander, "Internet of drones," *IEEE Access*, vol. 4, pp. 1148–1162, 2016.

[151] J. Wang, C. Jiang, K. Zhang, T. Q. Quek, Y. Ren, and L. Hanzo, "Vehicular sensing networks in a smart city: Principles, technologies and applications," *IEEE Wireless Commun.*, vol. 25, no. 1, pp. 122–132, Feb. 2018.

[152] L. Hanzo, H. Haas, S. Imre, D. O'Brien, M. Rupp, and L. Gyongyosi, "Wireless myths, realities, and futures: From 3G/4G to optical and quantum wireless," *Proc. IEEE*, vol. 100, pp. 1853–1888, May 2012.

[153] *Unmanned Systems Integrated Roadmap*, document 14-S-0553, Under Secretary Defense Acquisition, Technol. Logistics, 2015.

[154] M. T. Dabiri, S. M. S. Sadough, and M. A. Khalighi, "Channel modeling and parameter optimization for hovering UAV-based free-space optical links," *IEEE J. Sel. Areas Commun.*, vol. 36, no. 9, pp. 2104–2113, Sep. 2018.

CHAOXING YAN received the Ph.D. degree in communication and information system from the Beijing Institute of Technology, China, in 2012. In 2017, he was a Visiting Scholar with the Next-Generation Wireless Group chaired by Prof. Lajos Hanzo, School of Electronics and Computer Science, University of Southampton, U.K. Since 2012, he has been with the Beijing Research Institute of Telemetry, where he is currently a Senior Engineer and an Associate Project Manager. He has authored several scientific papers and is the holder of over 30 patents. His primary research interests include system integration and wireless techniques of UAV datalinks and networks, satellite communications, and space communication networking systems. He serves as the Session Chair of IEEE/CIC ICCC 2018 and a Reviewer of several IEEE journals.

LINGANG FU received the B.S. degree and the M.S. degree in communication and information system from the Harbin Institute of Technology, China, in 2003 and 2006, respectively. He has been with the Beijing Research Institute of Telemetry, since 2006, as a Senior Engineer and an Associate Project Manager. He has authored several patents. His research interests include system integration and wireless techniques of UAV communication, satellite communication, and satellite remote sensing systems.

JIANKANG ZHANG received the B.Sc. degree in mathematics and applied mathematics from the Beijing University of Posts and Telecommunications, in 2006, and the Ph.D. degree in communication and information systems from Zhengzhou University, in 2012. He was a Lecturer, from 2012 to 2013, and an Associate Professor, from 2013 to 2014, with the School of Information Engineering, Zhengzhou University. From 2009 to 2011, he was a Visiting Ph.D. Student with the School of Electronics and Computer Science, University of Southampton, U.K. From 2013 to 2014, he was a Postdoctoral Researcher with McGill University, Canada. He is currently a Senior Research Fellow with the University of Southampton. His research interests include wireless communications and signal processing, aeronautical communications, and broadband communications. Dr. Zhang was a recipient of a number of academic awards, including the Excellent Doctoral Dissertation of Henan Province, China, and the Youth Science and Technology Award of Henan Province, China. He serves as an Associate Editor for IEEE Access and a Guest Editor of a special issue on *EURASIP Journal on Advances in Signal Processing*.

JINGJING WANG received the B.S. degree (Hons.) in electronic information engineering from the Dalian University of Technology, Liaoning, China, in 2014, and the Ph.D. degree (Hons.) in information and communication engineering from Tsinghua University, Beijing, China, in 2019. From 2017 to 2018, he visited the Next Generation Wireless Group chaired by Prof. Lajos Hanzo, University of Southampton, U.K. He is currently a Postdoctoral Researcher with the Department of Electronic Engineering, Tsinghua University. His research interests include resource allocation and network association, learning theory aided modeling, analysis and signal processing, and information diffusion theory for mobile wireless networks. Dr. Wang received the China Postgraduate National Scholarship Award, in 2017, the Best Journal Paper Award from the IEEE Technical Committee on Green Communications and Computing, in 2018, the Beijing Distinguished Graduated Student Award, the Tsinghua Outstanding Distinguished Doctoral Dissertation, and the Best Paper Award from the IEEE ICC, in 2019.